The Effect of miR-338-3p as a Suppressor of Glioblastoma

by

James R. Howe VI

Neuroscience Honors Thesis
May 30, 2017
Department of Psychological and Brain Sciences
Dartmouth College

_____
Advisor: Bryan W. Luikart, Ph.D.

_____
Second Reader: Kyle S. Smith, Ph.D.

Abstract

MicroRNAs have been previously shown to play an important role in the regulation of neuronal development and neurogenesis in the dentate gyrus via modulation of gene expression. Prior experiments have determined that loss of miR-338-3p function in the dentate gyrus leads to the local gliomagenesis, and expression of miR-338-3p at low levels in clinical glioblastoma (GBM) is linked to a worse prognosis. In this study, we set out to examine how miR-338-3p acts as a tumor suppressor in GBM by interrogating its role in the development of dentate gyrus granule neurons and the proliferation of GBM cells. Using a retroviral sponge construct, we knocked down miR-338-3p *in vivo* exclusively in developing cells. When miR-338-3p was knocked down throughout development, granule neurons would sprout multiple primary dendrites, and primary dendrites would branch off of the soma in a disorganized manner. We created a miR-338-3p overexpression construct to assay its role in proliferation. When miR-338-3p is overexpressed in two separate miR-338-3p-deficient GBM cell lines *in vitro,* the proliferation rate of both cell lines decreases. When miR-338-3p is overexpressed in an *in vivo* allograft model of hippocampal GBM, it reduces tumor volume in an activity-dependent manner. These data identify miR-338-3p as a critical regulator of granule neuron development and as a potentially relevant tumor suppressor in glioblastoma.

Acknowledgments

First of all, I would like to thank Bryan Luikart for being such a great advisor to me over the past four years. I am very thankful for the opportunities he has given me in his lab ever since my first day in January 2014, allowing me to run experiments from the outset and entrusting me with a degree of autonomy that would be difficult to find anywhere else. It is impossible to overstate how much I appreciate his commitment to my growth as a scientist, providing me with consistent guidance and support, as well as an apparently inexhaustible patience. I would like to thank Stephanie Getz, Patrick Skelton, and Michael Williams for their theoretical and their technical expertise, their willingness to share their knowledge, and their eagerness and readiness to lend a helping hand when the going got tough. I would also like to express my appreciation to Gilbert Rahme for providing his materials and his expertise, Kyle Smith for serving as my second reader, and the Kaminsky Family Fund for financially supporting my research. Finally, I would like to express my gratitude to my father, without whom I would never have developed an initial interest in life sciences research in the first place.

Table of Contents

Figures

Introduction

MicroRNAs: A Paradigm Shift in Molecular Biology

For most of molecular biology's history, most researchers thought RNA had a single overarching function: take the information from DNA and make it into usable proteins. RNA usually transferred this information as mRNA and it also facilitated its translation into protein as rRNA or tRNA, but the overarching purpose remained the same. On December 3, 1993, two groups, led by Victor Ambros at Dartmouth and Gary Ruvkun at Harvard, simultaneously published the same groundbreaking discovery back-to-back in *Cell:* RNA can directly regulate other RNAs. Serendipitously, both groups independently performed similar experiments and made the same observation: the untranslated gene *lin-4* inhibited translation of the gene *lin-14* in developing *C. elegans* by binding a complementary sequence on the *lin-14* mRNA's 3' UTR as a short, single-stranded RNA transcript (Lee et al., 1993; Wightman et al., 1993). Seven years later, Gary Ruvkun's group discovered a second short regulatory RNA in *C. elegans*, *let-7*, followed by Victor Ambros's group identifying many more across multiple species, upon which they christened these RNAs as a new class of RNA, microRNAs (Lau et al., 2001; Lee and Ambros, 2001; Reinhart et al., 2000).

MicroRNAs (miRNAs) as a rule all operate in the manner described above. They bind complementary sequences in the 3' UTR of mRNA, post-transcriptionally regulating gene expression (Bartel, 2004). MiRNAs modulate expression of their target genes exclusively via downregulation, reducing protein expression but by no more than one-half in most cases (Baek et al., 2008). Most miRNAs downregulate hundreds of genes

(about half of the genome is predicted to be miRNA-regulated), powerfully influencing the proteome by mildly repressing expression on a grand scale (Selbach et al., 2008).

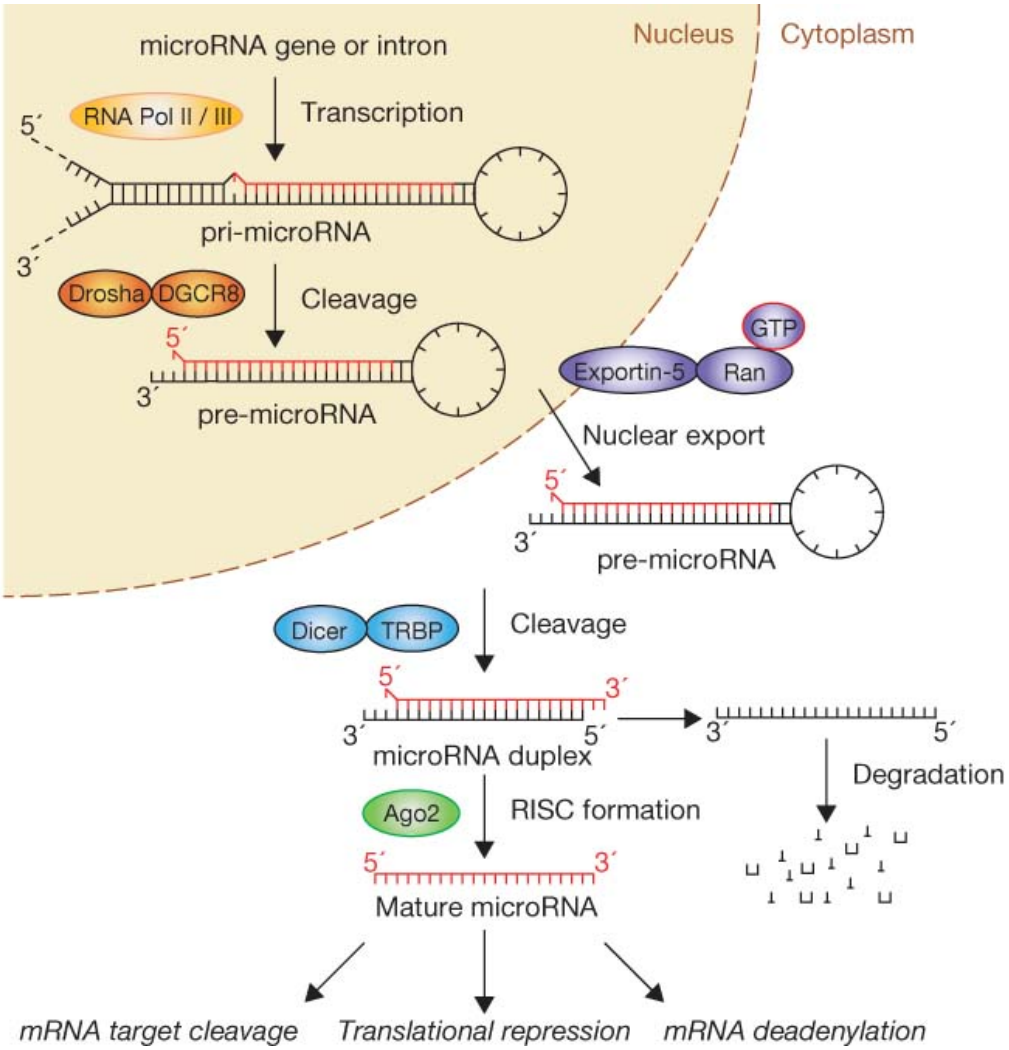

Figure 1. The canonical miRNA pathway. RNA pol II and III transcribe pri-miRNAs in the nucleus, which are cleaved into pre-miRNAs by an RNase-like Drosha/DGCR8 complex. Exportin-5 transports the pre-miRNA transcript out of the nucleus into the cytoplasm, where a Dicer/TRBP complex cleaves it into two mature miRNAs. The less stable strand is degraded, and the more stable strand then binds Ago2 in the RISC and guides the silencing of its target RNAs via cleavage, repression of translation, or removal of polyadenylation. Reproduced from (Winter et al., 2009).

To understand the importance of miRNAs, their biogenesis and function must be understood, summarized above in Figure 1. MiRNA genes tend to be located within intronic regions of the genome or antisense to exonic sequences. RNA polymerase II and

III transcribe miRNA genes in the nucleus into long primary precursor miRNAs, or pri-miRNAs, which form stem-loops based on partial self-complementarity (Borchert et al., 2006; Lee et al., 2004). While in the nucleus, a Drosha/DGCR8 ribonuclease (RNase) complex cleaves the pri-miRNA stem-loop, shortening the long pri-miRNA down to a 60-90 nt precursor miRNA, or pre-miRNA (Gregory et al., 2004; Lee et al., 2003). Exportin-5 then transports the pre-miRNA to the cytoplasm, where the RNase Dicer cleaves the stem-loop's loop, leaving a dsRNA duplex (Bernstein et al., 2001; Lund et al., 2004). This dsRNA is composed of two complementary strands, the -3p strand, the strand more proximal to the 3' end of the pre-miRNA, and the -5p strand, the strand more proximal to the 5' end. Both of these strands can function as miRNAs, but only one strand is selected, and the other is degraded based on 5' thermodynamic stability (Khvorova et al., 2003). The remaining strand is the mature miRNA, between 20-23 nt in length, with a modal length of 22 nt.

The mature miRNA downregulates its target miRNAs within the RNA-induced silencing complex (RISC), anchored by the RNase Ago2 (Liu et al., 2004). The miRNA guides the RISC by binding to miRNA response elements (MREs), complementary sequences in the 3' UTR of its target mRNAs. The miRNA generally binds partial complements in the MRE (and perfect complements, which are rare in animals), so long as its seed region, nt 2-7 counting from the mature miRNA's 5' end, pairs perfectly (Selbach et al., 2008). When the miRNA imprecisely pairs with the MRE, it either inhibits the target mRNA's translation or removes its polyadenylation followed by mRNA cleavage, and Ago2 directly cleaves the mRNA when perfect pairing does occur (Pasquinelli, 2012).

MiRNAs regulate a wide range of cellular processes, owing to their diverse targets. Some are of greater interest and applicability than others, though. Most miRNAs display highly diverse yet specific patterns of expression based on tissue type and developmental stage, establishing them as key regulators of development (Stefani and Slack, 2008). MiRNAs are especially enriched in the central nervous system (CNS) and their expression in the CNS is most strongly associated with synaptic plasticity, neurogenesis, and neurodevelopment (Kosik, 2006; Sun and Shi, 2015). As a result of their strong associations with these processes, miRNA-based therapies have recently attracted considerable attention as potential treatments for neurodevelopmental and neurodegenerative disorders, psychiatric disease, and cancer (Bader et al., 2011; Baumann and Winkler, 2014; Sun and Shi, 2015).

MiR-338-3p and its Role in the Central Nervous System

MiR-338 is one of the few miRNAs associated with all four of these types of disease. Gary Ruvkun's group identified miR-338 in 2004 from primary cultures of dissociated embryonic rat cortex *in vitro* and total RNA extracts of adult rat cortex *in vivo,* as part of the first study investigating neuron-enriched miRNAs (Kim et al., 2004). The *MiR338* gene, which encodes the pri-miR-338 sequence, resides within intron 8 of the Apoptosis Associated Tyrosine Kinase gene (*AATK)*. *MiR338* is part of a larger cluster of miRNA genes hosted within *AATK*, along with *MiR3065* on the other strand as its complement, *MiR657* and *MiR1250,* which respectively encode miR-3065, miR-657, and miR-1250. Of the two strands within the pre-miR-338 stem-loop, both 22 nt long, the -3p strand (hereafter referred to as miR-338-3p) predominates during strand selection,

while the -5p strand is usually not selected and subsequently degraded as the antisense strand. Some cells express miR-338-5p, but always at levels far lower than miR-338-3p.

Following its initial identification in the rat cortex, other groups identified the *MiR338* gene *in silico* in humans and mice based on genomic library sequence homology, and then *in vivo* studies verified its expression in both species shortly thereafter (Kim et al., 2004; Landgraf et al., 2007; Weber, 2005). Other studies have experimentally characterized miR-338-3p expression in rhesus macaques and zebrafish, and genomic sequences of at least 20 other investigated vertebrate species contain *MiR338* (Chen et al., 2005; Yue et al., 2008). No invertebrate or plant species' genomes contain *MiR338*. Within all vertebrate species carrying the *MiR338* gene, miR-338-3p's sequence is very highly conserved, which itself implies a strong functional role for the miRNA (Figure 2).

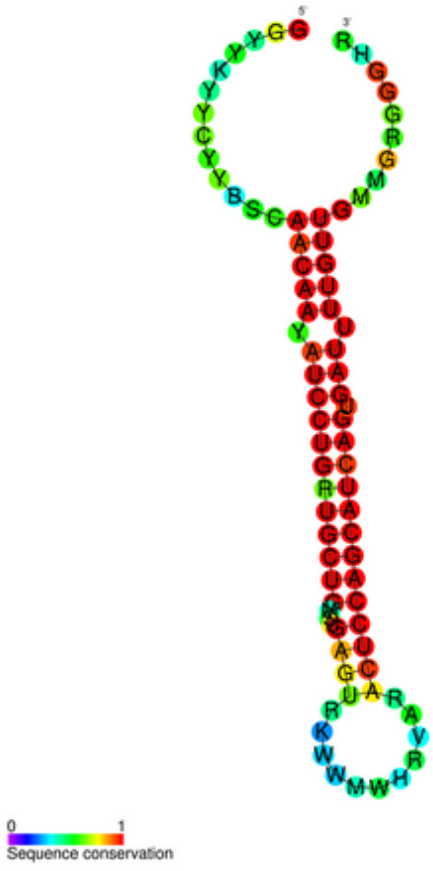

Figure 2. Pre-miR-338 sequence and its secondary structure. The pre-miR-338 sequence is imprecisely self-complementary, forming a stem-loop in its secondary structure. Individual bases are color-coded by their degree of sequence conservation across different species, in order of low to high conservation. The full mature miR-338-3p sequence is depicted (5'-UCCAGCAUCAGUGAUUUUGUUG-3'), and the entirety of the sequence is completely conserved across all studied vertebrate species. Reproduced from European Molecular Biology-European Bioinformatics Institute Rfam database (accession ID: RF00686).

MiRNAs of great functional importance tend to be expressed at high levels across a range of tissues within an organism (Chen and Rajewsky, 2007). MiR-338-3p generally follows this pattern, possessing a relatively ubiquitous but variable expression pattern within the tissues of most vertebrates. Human tissue samples of the gastric mucosa, liver, lung, and colon highly express miR-338-3p, and most other human tissues express the miRNA at moderate levels (Huang et al., 2009; Peng et al., 2014; Sun et al., 2015; Genotype-Tissue Expression Project, 2013; Xue et al., 2014). MiR-338-3p's expression pattern is most notable in the CNS. MiR-338-3p was originally discovered in total RNA extracts of rat cortex, and subsequent library analysis of total RNA extracts from various mouse tissues indicate strongest miR-338-3p expression in the brain as compared to other tissues (Chiang et al., 2010; Kim et al., 2004). RNA-seq data from the Genotype-Tissue Expression Project indicates variable miR-338-3p expression throughout the brain in normal human tissue: strong in the hypothalamus, amygdala, and cortex, among others, but rather weak in the basal ganglia and other structures (Genotype-Tissue Expression Project, 2013). At one point, miR-338-3p expression was so strongly associated with the CNS that an early study described it as a brain-specific miRNA (Aschrafi et al., 2008).

Genotype-Tissue Expression Project RNA-seq data also finds very high miR-338-3p expression in the human hippocampus (Genotype-Tissue Expression Project, 2013). Experiments performed by Sarah Streeter, a prior undergraduate in the lab, observed high

miR-338-3p expression in the murine dentate gyrus using a miR-338-3p-responsive sensor lentiviral construct (Figure 3, Howe et al., 2017)[1]. The sensor utilizes an mRNA transcript encoding mCherry, containing two perfectly complementary MREs for the miRNA of interest cloned into its 3' UTR (Figure 3A). If the infected cell expresses miR-338-3p, miR-338-3p will bind these MREs in *mCherry*'s 3' UTR, preventing its translation. In the absence of miR-338-3p, however, *mCherry* will translate to protein. Thus, the sensor reports the presence of miR-338-3p inversely: lower mCherry fluorescence indicates higher miR-338-3p expression, and vice versa. The miR-338-3p sensor fluorescence was compared to fluorescence in two other vectors. The first vector constitutively expressed mCherry, providing a relative baseline for fluorescence as a negative control (Figure 3B). The second vector expressed a similar sensor construct containing MREs for miR-137-3p, a miRNA highly expressed in the dentate gyrus, as a positive control (Figure 3C, Smrt et al., 2010). Under this assay, the miR-338-3p sensor exhibited very low fluorescence in the dentate gyrus relative to the control baseline, and both sensors exhibited comparable reductions in fluorescence (Figure 3D-E).

[1] Disclosure: I am the first author of this study.

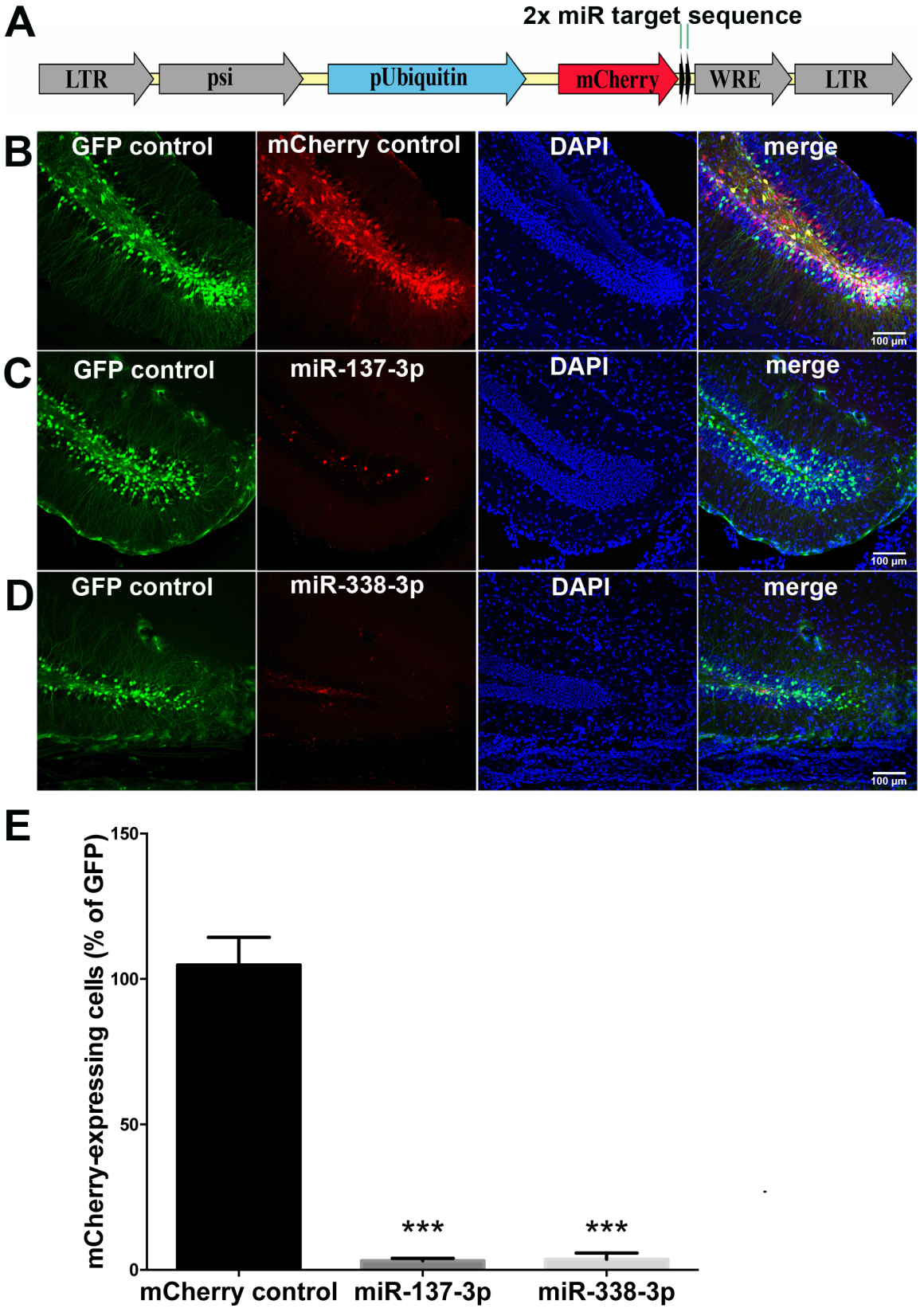
A
2x miR target sequence
LTR
psi
pUbiquitin
mCherry
WRE
LTR
B
GFP control
mCherry control
DAPI
merge
100 µm
C
GFP control
miR-137-3p
DAPI
merge
100 µm
D
GFP control
miR-338-3p
DAPI
merge
100 µm
E
mCherry-expressing cells (% of GFP)
150
100
50
0
***
***
mCherry control
miR-137-3p
miR-338-3p

Figure 3. *In vivo* detection of miR-338-3p in the dentate gyrus using an mCherry sensor. A. Construction of the lentiviral vector, using an FUCW backbone and two target-complementary sequences immediately downstream of mCherry. **B.** Co-injection of control GFP-expressing and mCherry-expressing viruses (equal titer) into the dentate gyrus of adult mice results in roughly equal infection rates; sections counter-stained with DAPI, which stains cell nuclei. **C.** Co-injection of the miR-137-3p sensor lentiviral construct and control GFP-expressing virus. **D.** Co-injection of miR338-3p sensor and control GFP-expressing virus. **E.** Expression levels of miR-137-3p and miR-338-3p in the dentate gyrus relative to control mCherry-expressing vector. ***$p<0.001$. Graph shows mean ± SEM. Adapted from (Howe et al., 2017).

These data clearly indicate miR-338-3p is highly expressed in the murine dentate gyrus. Within the dentate gyrus, miR-338-3p appears to be regulated in an activity-dependent manner. RNA expression microarray assays detect increased miR-338-3p expression shortly after pilocarpine infusion, indicating high neuronal activity in the dentate gyrus upregulates miR-338-3p expression (Luikart et al., 2012). However, the specific mechanism by which neuronal activity upregulates miR-338-3p expression remains unknown. At this time, only two specific mechanisms for regulation of miR-338-3p expression have been described, but neither have yet been observed in the CNS. First, methylation of a CpG island within the upstream *MiR338* promoter can epigentically silence miR-338-3p expression in human gastric tissue by recruiting MECP2 to this promoter to repress miR-338-3p expression (Li et al., 2013; Tong et al., 2016). Second, the mineralocorticoid receptor binds the *MiR338* promoter *in vitro* in hepatocellular carcinoma cell lines, upregulating transcription of the pri-miR-338-3p sequence (Nie et al., 2015). Determination of whether these mechanisms regulate miR-338-3p expression within the overall CNS or within the dentate gyrus in particular requires further research. Additionally, more regulatory mechanisms almost certainly remain unknown, which would provide a much better understanding of miR-338-3p if discovered.

Increasing neuronal activity upregulates many phenomena in the dentate gyrus, not just miR-338-3p expression. Inducing high levels of neuronal activity via pilocarpine-induced seizures also sharply increases neurogenesis, a phenomenon largely confined to the dentate gyrus in adults, whereby neural stem cells differentiate into mature neurons (and oligodendrocytes or astrocytes), and integrate into existing networks (Parent, 2007). The dual association of this pilocarpine-induced seizure model with both miR-338-3p upregulation and neurogenesis points to a potential association between the two. To this end, prior students in the laboratory performed experiments examining miR-338-3p expression in neurons at varying stages of maturity by examining co-expression of the mCherry sensor with neuronal maturity-specific biomarkers (Howe et al., 2017). They stained for three biomarkers: Nestin, an intermediate filament protein expressed by neural progenitor cells, doublecortin, a microtubule-associated protein expressed by neuronal precursor cells and newly differentiated neurons, and NeuN, a neuronal nuclear antigen expressed exclusively by mature neurons. Co-expression of the mCherry sensor was then normalized to a control mCherry signal. Fluorescence of the mCherry miR-338-3p sensor at each point in maturity was compared to the fluorescence of a similar sensor containing MREs specific to miR-132-3p, a previously-characterized miRNA expressed throughout dentate gyrus neurogenesis, but most highly in mature neurons (Luikart et al., 2011).

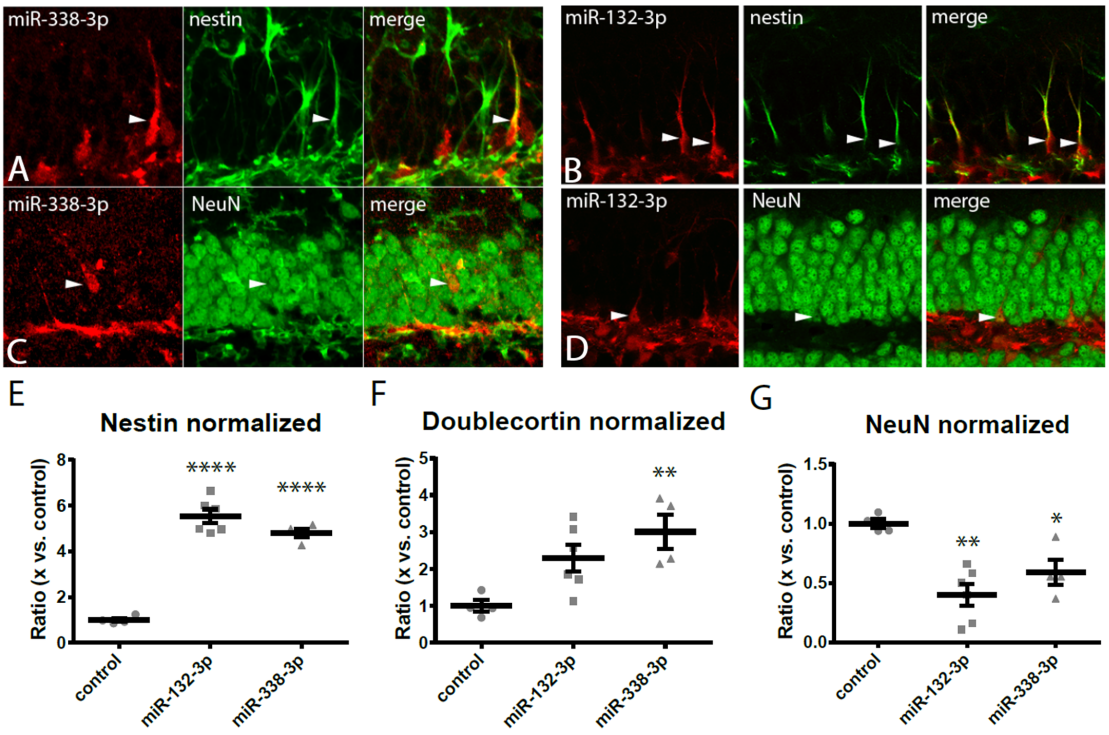

Figure 4. MiR-338-3p expression increases with maturity in dentate gyrus granule neurons. A. Co-localization of nestin (arrowheads) with miR-338-3p sensor. **B.** Co-localization of nestin (arrowheads) with miR-132-3p sensor. **C.** Co-localization of NeuN (arrowheads) and miR-338-3p sensor. **D.** Co-localization of NeuN (arrowheads) and miR-132-3p sensor. **E.** Ratio of cells co-labeled with either the miR-338-3p or miR-132-3p sensor and nestin as compared to control mCherry virus. **F.** Ratio of cells co-labeled with either the miR-338-3p or miR-132-3p sensor and doublecortin as compared to control mCherry virus. **G.** Ratio of cells co-labeled with either the miR-338-3p or miR-132-3p sensor and NeuN as compared to control mCherry virus. *p<0.05, **p<0.01, ****p<0.0001; Graphs show mean ± SEM. Adapted from (Howe et al., 2017).

A clear pattern emerges from observed co-expression. Neural progenitor cells display very low levels of miR-338-3p expression, as shown by high mCherry fluorescence co-localizing with nestin (Fig 4E). The same holds true for immature neurons as well (Figure 4F). However, very low levels of mCherry were detected co-localized with NeuN, indicating high miR-338-3p expression in mature neurons (Figure 4G). Thus, miR-338-3p expression appears to increase with increasing maturity in dentate gyrus granule neurons, and this proposition is strengthened by miR-132-3p

displaying the exact same pattern. While this experiment shows miR-338-3p expression increases as maturity increases, it does not conclusively indicate that miR-338-3p is actually involved in maturation of developing granule neurons in the dentate gyrus. For example, maturity-associated processes could upregulate miR-338-3p, without it having an effect in and of itself, among other possibilities. However, miR-338-3p does have strong functional effects in the CNS, as discussed in the next section.

The Role of miR-338-3p in the Central Nervous System

The first papers discussing miR-338-3p in neural development concerned themselves with its role in axonal outgrowth. A series of *in vitro* studies utilizing primary cultures of rat sympathetic superior cervical ganglion neurons indicated miR-338-3p expression rises in the axon as the neuron matures, its localization dependent on axonal trafficking of the pre-miR-338 transcript (Aschrafi et al., 2008; Vargas et al., 2016). MiR-338-3p overexpression and knockdown experiments in rat cortical and superior cervical ganglion cells provided evidence arguably expanding miR-338-3p's role to most other neurons, finding miR-338-3p attenuates axonal outgrowth in these neurons *in vitro* (Aschrafi et al., 2012; Kos et al., 2016). The investigators further described a number of potential mechanisms with explanatory power. First, pre-miR-338 can localize to the axonal mitochondria, allowing miR-338-3p to repress expression of multiple genes encoding cytochrome c oxidase and ATP synthase (e.g. *COXIV, ATP5G1, ATP5B)*, the two final complexes in the electron transport chain, leading to reductions in local oxidative phosphorylation at the axon, impairing outgrowth (Aschrafi et al., 2012; Aschrafi et al., 2008; Vargas et al., 2016). Second, miR-338-3p represses expression of

Robo2, a gene encoding a receptor crucial for guidance and growth of the axon (Kos et al., 2016). Third, miR-338-3p represses its host gene, *AATK,* which works through a variety of pathways to regulate neurite outgrowth, but the precise changes and the specific molecular mechanisms responsible are still heavily disputed (Barik, 2008; Kos et al., 2012). However, all of these studies only use *in vitro* methods. Even though primary cultures were used, the relationship between miR-338-3p and axonal outgrowth still requires validation *in vivo* before it can possess explanatory power.

Recently, miR-338-3p has emerged as a potential inhibitor of schizophrenia. Human dorsolateral prefrontal cortex tissue isolated postmortem from schizophrenics display downregulated miR-338-3p expression levels (Moreau et al., 2011). Further, mouse models of 22q11.2 deletion syndrome, a developmental disorder highly co-morbid with schizophrenia, both display canonical markers of schizophrenia like poor prepulse inhibition and disrupted thalamocortical transmission while expressing miR-338-3p at decreased levels throughout the prefrontal cortex and thalamus (Chun et al., 2017; Stark et al., 2008). MiR-338-3p overexpression rescued these schizophrenia-related deficits, while loss of miR-338-3p function alone was sufficient to induce them (Chun et al., 2017). Early mechanistic explanations focus on miR-338-3p's regulation of *Drd2*, a gene upregulated in schizophrenia encoding a dopamine receptor, which is inhibited by antipsychotics (Chun et al., 2017). While this hypothesis appears compelling, the association between miR-338-3p is currently contested, with another study reporting upregulation of miR-338-3p in the postmortem prefrontal cortex of schizophrenia patients (Beveridge et al., 2010). More research is required to validate the protective effect of miR-338-3p against schizophrenia and determine other potential underlying mechanisms.

The best-validated function of miR-338-3p in the CNS takes place in oligodendrocytes, which myelinate CNS neurons. MiR-338-3p expression in oligodendrocytes across maturation closely matches that of granule neurons: miR-338-3p expression is very low in rodent oligodendrocyte precursor cells (OPCs) *in vivo* and *in vitro*, but increases as the cell matures, reaching high levels of expression in mature oligodendrocytes (Dugas et al., 2010; Lau et al., 2008). Knockdown of miR-338-3p *in vivo* and *in vitro* prevents murine OPCs from differentiating into mature oligodendrocytes and *in vivo* and *in vitro* miR-338-3p overexpression in murine OPCs will cause them to differentiate into oligodendrocytes, proving miR-338-3p is both sufficient and necessary for differentiation of OPCs into oligodendrocytes (Diao et al., 2015; Ebrahimi-Barough et al., 2013; Zhao et al., 2010). MiR-338-3p expression likely regulates OPC differentiation by repressing the translation of *Sox6* and *Hes5*, which both inhibit OPC differentiation and likely contain MREs for miR-338-3p, with 3' UTRs that bind miR-338-3p *in vitro* (Zhao et al., 2010). MiR-338-3p's role in OPC differentiation is of potential clinical significance: demyelinating lesions in multiple sclerosis tend to express miR-338-3p at low levels and miR-338-3p displays the same maturity-specific expression pattern in isolated human oligodendrocytes (de Faria Jr. et al., 2012; Junker et al., 2009).

The similar maturity-associated expression pattern of miR-338-3p in both granule neurons and oligodendrocytes suggests that this miRNA could have the same strong functional effect in the former as seen in the latter. To evaluate the function of miR-338-3p *in vivo*, Emily Li, a prior undergraduate in the laboratory, generated a lentiviral sponge construct to reduce activity of miR-338-3p by binding it and preventing the miRNA from interacting with its endogenous targets, effectively sequestering it (Howe et

al., 2017). The sponge contains 6 target MREs for miR-338-3p downstream from both the U6 and H1 promoters, for a total of 12 sponge MREs. The sponge also contains the previously described sensor cassette with 2 MREs in *GFP*'s 3' UTR driven by a ubiquitin promoter, granting simultaneous knockdown and detection of miR-338-3p expression *in vivo* (Figure 5A). The miR-338-3p sponge-infected cells highly express the GFP sensor, comparable to a co-injected mCherry-only control of equal titer, validating that the sponge knocks down miR-338-3p effectively in infected cells (Figure 5B, 5C).

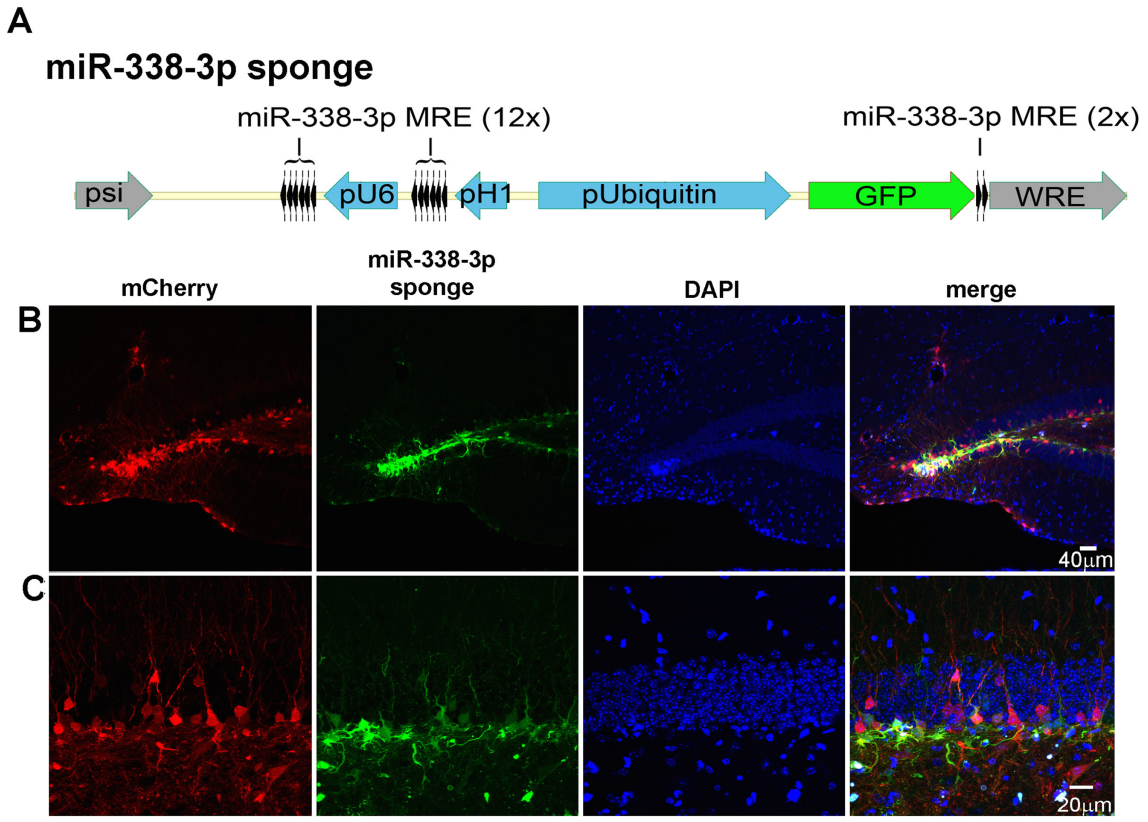

Figure 5. *In vivo* verification of miR-338-3p sponge efficacy and initial identification of cell clusters. A. Design of lentiviral miR-338-3p sponge with a sensor cassette. The miR-338-3p sensor cassette contains 2 perfectly complementary miR-338-3p target sequences downstream of GFP driven by the pUbiquitin promoter and the sponge cassette consists of 6 targets downstream of both the H1 and U6 promoters for a total of 2 sensor targets to sense miR-338-3p activity and 12 sponge targets to sequester endogenous miR-338-3p. **B.** Low magnification images of dentate gyrus show the mCherry control and the miR-338-3p sponge exhibit similarly high levels of expression. **C.** Images from 5B, but under high magnification. This demonstrates the ability of the sponge cassette to

sequester ligand away from the miR-338-3p targets expressed in the sensor cassette. Reproduced from (Howe et al., 2017).

The most noticeable effect of the sponge became immediately apparent. In multiple mice infected with the sponge virus, small neoplastic clusters of cells arose locally, displaying reduced organization compared to the surrounding tissue (Figure 5B). Determination of miR-338-3p's function in our laboratory then shifted toward a potential link between loss of miR-338-3p expression and the observed neoplastic cells, and by extension, potential future tumors. Follow-up experiments set out to determine whether these regions of neoplasia induced by miR-338-3p could indeed be a precursor to cancer.

MiR-338-3p as a General Tumor Suppressor MiRNA

Since the 1970s, a great deal of cancer research has been performed within the paradigm of oncogenes and tumor suppressor genes. Oncogenes broadly upregulate processes contributing to proliferation (i.e. mitosis, cell cycle progression) or downregulate anti-proliferative processes (i.e. differentiation, apoptosis), where gains in function based on increased expression or activity level result in cancer (Nishimura and Sekiya, 1987). Tumor suppressor genes oppose oncogenes, downregulating mitosis and cell cycle progression, while maintaining or inducing differentiation and apoptosis; cancer can arise through loss of their function (Marshall, 1991). MiRNAs can act in a similar manner to oncogenes and tumor suppressor genes, but are instead referred to as oncomiRs and tumor suppressor miRNAs, respectively. Tumor suppressor miRNAs, like tumor suppressor genes, repress expression of oncogenes and/or regulate cellular differentiation, proliferation, or apoptosis (Zhang et al., 2007). A tumor suppressor miRNA only needs to regulate one of these processes or one such oncogene to qualify

(usually they regulate a process by repressing one or more oncogenes, but not always), so long as it inhibits oncogenesis. However, due to the vast number of genes most miRNAs regulate, many tumor suppressor miRNAs regulate most, if not all of these processes.

Joshua Mendell, one of the first researchers studying the relationship between miRNAs and cancer, proposed a useful and widespread validation framework for determining whether a miRNA of interest acts as an oncomiR or a tumor suppressor miRNA (Kent and Mendell, 2006). First, the miRNA is dysregulated in a diverse set of cancers in the clinic. Second, genome sequencing of clinical tumors turns up at least one gain- or loss-of-function genotype in the miRNA. Third, the miRNA's oncogenic or tumor-suppressing properties can be recapitulated in an animal model *in vivo.* The fourth and final criterion requires determination of a mechanism through which the miRNA causes its effect, ideally including identification of a specific molecular pathway or target known to cause that effect. Not all oncomiRs or tumor suppressor miRNAs have been validated under all four criteria, but they generally do fulfill at least three of the listed criteria. Prior studies have provided sizeable evidence that miR-338-3p functions as a tumor suppressor miRNA, fulfilling three of Mendell's four criteria. The remainder of this section looks into these studies and how miR-338-3p fulfills these criteria outside of the nervous system, reviewing miR-338-3p's general role as a tumor suppressor miRNA, the overarching concern for most of the extant miR-338-3p literature.

The first clinical identification of differential miR-338-3p expression in cancer was conducted and subsequently verified multiple times in hepatocellular carcinoma, a form of liver cancer common in developing countries, where the miRNA is consistently underexpressed in tumor biopsies compared to adjacent liver tissue (Huang et al., 2009;

Xu et al., 2014; Zhang et al., 2016b). This expression pattern was soon observed again and again across a diverse range of other forms of carcinoma, the types of cancer derived from cells in the epithelial lineage. Other tissues where miR-338-3p is downregulated in carcinoma include the lung, prostate, nasopharynx and breast (Bakkar et al., 2016; Jin et al., 2015; Shan et al., 2015; Sun et al., 2015). The same holds true for carcinomas found throughout the majority of the gastrointestinal tract, specifically in the mouth, esophagus, stomach, and rectum (Gaedcke et al., 2012; Li et al., 2013; Lin et al., 2012; Scapoli et al., 2010). Groups have also observed low miR-338-3p expression in tumors not derived from epithelial tissue, like ovarian cancer and melanoma (Caramuta et al., 2010; Zhang et al., 2016c). MiR-338-3p downregulation in a variety of cancers in such a broad and diverse range of tissues establishes it as a potential tumor suppressor, fulfilling the first of Mendell's criteria.

The link between miR-338-3p and some of these cancers is so strong, in fact, that miR-338-3p expression could be used as a prognostic biomarker in the clinic. MiR-338-3p expression level in tumor biopsies is negatively correlated with many prognostic factors in carcinomas (stomach, esophagus, prostate, liver and lung), including but not limited to tumor size, metastasis, and aggression (Bakkar et al., 2016; Huang et al., 2009; Li et al., 2013; Sun et al., 2015; Yang et al., 2013). The degree of miR-338-3p downregulation alone in prostate tumors and in combination with other miRNAs in esophageal and gastric tumors predicts reduced five-year survival (Bakkar et al., 2016; Li et al., 2010; Wu et al., 2013). Circulating miR-338-3p levels exhibit the same relationship in oral carcinoma, where low expression correlates with cancer prognosis, but the inverse is true for carcinoma of the breast and liver, paradoxically, reducing the biomarker's

potential utility (Kodahl et al., 2014; Maclellan et al., 2012; Zhang et al., 2011). Preliminary studies indicate miR-338-3p expression may predict response in different carcinomas to various compounds used in chemotherapy (Wu et al., 2011; Xu et al., 2014). The myriad links between miR-338-3p expression and various prognostic factors for many forms of cancer provides strong evidence for miR-338-3p as a tumor suppressor and indicates that measuring miR-338-3p expression is of potential clinical significance.

Mendell's second criterion is more exacting, requiring sequencing of human tumor biopsies to determine changes to the *MiR338* sequence. No studies published thus far have examined *MiR338* deletions or mutations using cancer genome sequencing or more focused assays. Multiple databases report one copy number variant and multiple single nucleotide polymorphisms in *MiR338*, but the effect of these elements with regard to cancer susceptibility has not yet been studied. This is clearly an understudied aspect of miR-338-3p, and research into miR-338-3p does not satisfy this second criterion, which is fertile ground for further experiments.

Mendell's third criterion calls for *in vivo* studies recapitulating the tumor suppressing properties of the miRNA. While *in vivo* studies exist, investigators have only performed them in a limited set of very similar models. In these models, the investigators xenografted tumor cells overexpressing miR-338-3p into immunosuppressed mice, then harvested tumors and measured miR-338-3p's effects on tumorigenicity. Using this model, multiple groups determined miR-338-3p's inhibitory effect on tumor proliferation in hepatocellular carcinoma xenografted subcutaneously and orthotopically, while also sensitizing these tumors to sorafenib, a chemotherapeutic used to treat hepatocellular carcinoma (Chen et al., 2016; Xu et al., 2014). Multiple studies similarly confirmed miR-

338-3p's inhibitory effect on tumorigenicity in gastric cancer cells xenografted into nude mice by inhibiting cellular proliferation and upregulating apoptosis (Guo et al., 2014; Li et al., 2013; Peng et al., 2014). MiR-338-3p putatively exerts a similar effect in breast cancer and non-small-cell lung carcinoma each based on results from a single study, where miR-338-3p expression inhibited tumor cell proliferation in similar nude mouse subcutaneous xenograft models (Jin et al., 2015; Zhang et al., 2017). These experiments are a start, but require replication to ensure validity. Additionally, many other forms of cancer displaying low miR-338-3p expression still need to be validated *in vivo*. More diverse models utilizing different species, miR-338-3p knockdown, and/or non-xenografted tumors would be constructive and add a great deal of validity by minimizing potential confounding variables arising from these xenograft models.

Mendell's fourth criterion asks for a validated mechanism by which the miRNA could suppress carcinogenesis, examining the miRNA's effects on specific phenomena within the cell. These mechanisms generally, but not always, involve a molecular target of the miRNA that could induce carcinogenesis if its miRNA-mediated repression is lost. Proliferation, differentiation, and apoptosis are the three mechanisms of primary interest, because these three processes are themselves sufficient to induce carcinogenesis (Luch, 2005). Other miRNA-regulated processes may be associated with cancer and various phenotypes of cancer, but by themselves are not carcinogenic.

As stated in the discussion of Mendell's third criterion, most *in vivo* studies thus far have examined the role of miR-338-3p in the cellular proliferation. *In vitro* studies have recapitulated these results many times over, using a diverse range of methods. Increased miR-338-3p expression inhibits proliferation in multiple assays using cancer

cell lines modeling nearly every form of cancer linked to reduced miR-338-3p expression (Guo et al., 2014; Jin et al., 2015; Li et al., 2013; Liu et al., 2015; Peng et al., 2014; Sun et al., 2015; Sun et al., 2013; Yan et al., 2017; Zhang et al., 2017; Zhang et al., 2016c). To a lesser degree, this same phenomenon has been confirmed via miR-338-3p inhibition, which increases proliferation in multiple cell lines from carcinomas derived from the gastrointestinal tract (Guo et al., 2014; Sun et al., 2013; Yan et al., 2017). Two molecular targets have been investigated based on their association with cellular proliferation. The first is *Cdk4,* which induces G_1-S arrest in the cell cycle, increasing cell cycle length and inhibiting proliferation (Duan et al., 2017). The second is *SOX4*, a transcription factor regulating expression of multiple genes involved in various aspects of proliferation (as well as differentiation and apoptosis, but these mechanisms are currently theoretical in miR-338-3p-related tumorigenesis), which is both directly regulated by miR-338-3p and downregulated in quickly-proliferating miR-338-3p deficient tumors (Jin et al., 2015).

The next-best investigated mechanism of the three mechanisms is miR-338-3p's regulation of apoptosis. As a tumor suppressor, miR-338-3p is expected to induce and/or maintain apoptosis in aberrant cells. When miR-338-3p is overexpressed *in vitro* in multiple cancer cell lines from colorectal, hepatocellular, non-small cell lung, gastric and breast cancers, apoptosis is upregulated (Guo et al., 2014; Jin et al., 2015; Li et al., 2013; Peng et al., 2014; Sun et al., 2015; Sun et al., 2013; Xu et al., 2014; Yan et al., 2017; Zhang et al., 2017). Conversely, inhibition of miR-338-3p expression in esophageal and colorectal carcinoma cells *in vitro* reduces their relative frequency of apoptosis (Sun et al., 2013; Yan et al., 2017). Like its anti-proliferative effect, miR-338-3p's pro-apoptotic effect has been observed *in vivo,* albeit again in a single study (Li et al., 2013). Most

molecular mechanisms relating to miR-338-3p's pro-apoptotic effect are generally involved in cancer-related processes and not specific to apoptosis. The only molecular target examined solely for its relationship to apoptosis is *HIF-1α*, a transcription factor overexpressed in many cancers. MiR-338-3p directly binds the *HIF-1α* 3' UTR and inhibits its expression; *HIF-1α* both independently downregulates apoptosis and counteracts the pro-apoptotic effect of miR-338-3p overexpression in hepatocellular carcinoma cells (Xu et al., 2014).

The third and final primary carcinogenic mechanism is miR-338-3p's regulation of cellular differentiation, which is by far the least well studied of the three. Here, no prior *in vivo* studies have been performed. Outside the nervous system, the only known role of miR-338-3p in cellular differentiation is in establishing the epithelial phenotype. MiR-338-3p is expressed at a much higher level in differentiated than undifferentiated epithelial cells *in vitro*, and it acts in conjunction with miR-451 to induce epithelial polarization (Tsuchiya et al., 2009). MiR-338-3p similarly inhibits the epithelial to mesenchymal transition (EMT), a normal developmental process found ubiquitously in metastatic cancer, where tightly adhering, static, polar epithelial cells develop into loosely adherent, motile, nonpolar mesenchymal cells, generally through upregulation of Akt pathway signaling (Larue and Bellacosa, 2005). Inhibition of miR-338-3p expression in hepatocellular carcinoma and gastric cancer cells is sufficient to induce the EMT both *in vitro* and *in vivo,* upregulating mesenchymal biomarkers (e.g. vimentin, Snail1) and downregulating E-cadherin, an epithelial biomarker and tumor suppressor, while adopting mesenchyme-like morphology (Chen et al., 2016; Huang et al., 2015; Peng et al., 2014). All molecular mechanisms for miR-338-3p to regulate differentiation do so

through the Akt pathway. One primary candidate is *MACC1,* a metastasis-associated oncogene that indirectly upregulates Akt signaling, and is directly inhibited by miR-338-3p (Huang et al., 2015). *MACC1* overexpression upregulates vimentin expression, downregulates E-cadherin expression, and increases cancer cell motility, and maintains a mesenchymal phenotype despite miR-338-3p overexpression (Huang et al., 2015).

MiR-338-3p also regulates other auxiliary processes that affect cancer cells' ability to thrive and metastasize beyond direct tumorigenesis. The best validated are cell migration and invasion, the ability for cancer cells to move to other tissues and infiltrate them, respectively, which facilitate tumor metastasis. Loss of miR-338-3p expression drastically increases both processes in a diverse range of cancer cell lines *in vitro*, and induction of miR-338-3p expression has the converse effect (Chen et al., 2016; Huang et al., 2015; Huang et al., 2011; Jin et al., 2015; Li et al., 2013; Liu et al., 2015; Peng et al., 2014; Xue et al., 2014). MiR-338-3p expression reduces angiogenesis in multiple cancers *in vivo* and *in vitro*, the process by which tumors recruit new blood vessels to facilitate growth; corresponding loss of miR-338-3p expression results in increased vascularization of cancer tissue (Peng et al., 2014; Zhang et al., 2016b). Further, miR-338-3p loss-of-function *in vitro* induces the Warburg effect, a process ubiquitous in cancer where cells switch from aerobic respiration to lactate fermentation, by upregulating *PKM2* and *PKLR* (Nie et al., 2015; Zhang et al., 2016c). These two genes encode pyruvate kinases directly suppressed by miR-338-3p that catalyze lactate fermentation; restoring their inhibition is sufficient to reverse the Warburg effect in some cancer cell lines.

Two molecular targets of miR-338-3p have more general effects across a range of these phenomena. Neuropilin-1 (*NRP1)* is a co-receptor for many cell-surface receptors

involved in a wide range of general signaling pathways (e.g. MAPK, Akt) regulating a great deal of cellular phenomena related to cancer, including but not limited to apoptosis, differentiation, and angiogenesis (Peng et al., 2014). Overexpression of *NRP1* is sufficient to counteract miR-338-3p overexpression's inhibitory effect on migration, invasion, EMT, and proliferation, as well as its upregulation of apoptosis (Liu et al., 2015; Peng et al., 2014). *In vivo* overexpression of *NRP1* in gastric tumors prevents miR-338-3p overexpression from inhibiting proliferation and angiogenesis (Peng et al., 2014). MiR-338-3p directly inhibits expression of the oncogene smoothened (*SMO)*, which mediates all signaling through the hedgehog pathway, a signaling pathway regulating a range of diverse functions, including all three major processes contributing to carcinogenesis. Inhibition of *SMO* expression in cancer cell lines produces identical inhibitory effects on proliferation and migration to those observed as a result of miR-338-3p expression, and its overexpression is sufficient to rescue upregulation of proliferation and migration resulting from miR-338-3p knockdown in cancer cells (Huang et al., 2011; Sun et al., 2013; Xue et al., 2014). Hedgehog signaling also plays a role in the EMT, and inhibition of *SMO* expression prevents miR-338-3p knockdown from inducing the EMT in hepatocellular carcinoma (Chen et al., 2016).

Of special note is the long non-coding RNA Snhg1, which is not translated into protein and has no known cellular function, but serves as a prognostic biomarker for multiple cancers associated with miR-338-3p loss and somehow promotes proliferation and inhibits apoptosis in hepatocellular and esophageal carcinoma cell lines (Yan et al., 2017; Zhang et al., 2016a). Interestingly, Sngh1 can bind miR-338-3p without being degraded, decreasing its functional expression and acting as a physiological sponge;

expression of Snhg1 is sufficient to override the anti-proliferative and pro-apoptotic effects of miR-338-3p overexpression in esophageal cancer cell lines (Yan et al., 2017).

MiR-338-3p clearly acts as a general tumor suppressor throughout the body, fulfilling three of Mendell's four criteria. Numerous research groups systematically observe low miR-338-3p expression across a wide range of cancers, to the degree that miR-338-3p expression has prognostic power. Animal models confirm the association between loss of miR-338-3p function and tumorigenesis *in vivo.* Multiple tumor suppression mechanisms and associated molecular targets for miR-338-3p have been validated across a large subset of these cancers using an array of methods. The primary gap in the literature thus far is in what Mendell lists as his second criterion: no specific miR-338-3p mutations or variants have been identified that cause or predispose to cancer. In the following section, miR-338-3p's effects as a tumor suppressor miRNA in the nervous system will be reviewed in greater detail.

MiR-338-3p as a Tumor Suppressor in the Nervous System

Compared to the literature outside the nervous system, studies of miR-338-3p as a tumor suppressor within the nervous system are relatively sparse. All of the literature thus far has focused on two general classes of cancer within the nervous system. The first is neuroblastoma (NB), a relatively rare type of tumor taking root in early childhood, arising from stem cells in the developing sympathetic nervous system and subsequently manifesting as tumors in the adrenal glands and sympathetic ganglia (Matthay et al., 2016). The first study documenting miR-338-3p dysregulation in nervous system cancers focused on its expression in NB biopsies and cell lines (Ragusa et al., 2010).

Surprisingly, their observations ran counter to all other groups up to this point: clinical NB samples and corresponding NB cell lines appeared to express miR-338-3p at high levels compared to adrenal tissue, conferring protection against apoptosis.

The few other papers following up on miR-338-3p in NB strongly disputed these findings, however. An initial microarray study of miRNAs and its more focused follow-up on miR-338-3p found downregulation of miR-338-3p in animal models of metastatic NB as well as human clinical NB biopsies (Chen et al., 2013; Guo et al., 2010). The experiments in the follow-up supported the 'orthodox' view of miR-338-3p as a tumor suppressor, directly contradicting the earlier group: miR-338-3p knockdown stimulated increased proliferation, migration, invasion, and cell viability in multiple NB cell lines *in vitro*, while miR-338-3p overexpression inhibited all of these same phenomena (Chen et al., 2013). Furthermore, the group identified a molecular target in *PREX2a,* which encodes a protein that inhibits PTEN, a phosphatase that negatively regulates Akt signaling and is a well-characterized tumor suppressor (Fine et al., 2009). Along with an earlier study in gastric cancer, they found miR-338-3p directly binds the *PREX2a* 3' UTR and represses its expression; they observed *PREX2a* knockdown induces the same upregulation of proliferation and invasion in NB as miR-338-3p overexpression (Chen et al., 2013; Guo et al., 2014). Finally, they were able to prove that miR-338-3p knockdown mediates its effect at least partially via *PREX2a,* because *PREX2a* knockdown was sufficient to override the effects of miR-338-3p knockdown, retaining its upregulated proliferation and invasion (Chen et al., 2013). From these results, while more research may be required, miR-338-3p likely acts as a tumor suppressor miRNA for NB as well, despite earlier evidence in opposition.

All other studies of miR-338-3p expression in nervous system tumors have looked at miR-338-3p expression in glioma. Glioma is a class of tumors thought to arise from glial cells and their precursors, displaying glial histology and biomarkers like glial fibrillary astrocytic protein (GFAP), an astrocyte-specific protein (Furnari et al., 2007). Gliomata are the most common type of brain tumor, are by far the most malignant, and are responsible for the majority of deaths resulting from primary brain tumors (Weller et al., 2015). Gliomata are defined and further subdivided into four grades by a standard classification based on their histology and biomarker expression, which reflect different general prognoses for each (Louis et al., 2016). The least malignant gliomata are graded I or II and known as low-grade gliomata. The more malignant gliomata are called high-grade gliomata and given a grade of III or IV. Grade IV glioma is more widely known as glioblastoma (GBM), the most common, lethal, and malignant form of glioma, with the worst prognosis (Weller et al., 2015). GBM has a very distinctive histology chacterized by two vastly different regions: a core intratumoral region, and a marginal peritumoral region. The intratumoral region is characterized by wide necrosis and de-differentiation, while the peritumoral region is highly proliferative (Aldape et al., 2015).

Mendell's criteria can be used as a framework to evaluate the evidence for miR-338-3p as a suppressor of glioma. MiR-338-3p's downregulation in glioma is well-validated, fulfilling the first criterion. MiR-338-3p is consistently underexpressed across all four WHO grades of glioma, in both human clinical glioma biopsies and human glioma-derived cell lines (Ames et al., 2017; Lavon et al., 2010; Rao et al., 2010; Shang et al., 2016). In fact, the level of miR-338-3p expression can be used as a prognostic biomarker for GBM. GBM patients with a primary tumor expressing miR-338-3p in the

bottom 30th percentile survive much shorter than patients with a primary tumor highly expressing miR-338-3p, and their cancer progresses more aggressively, proliferating and invading other tissues more quickly (Howe et al., 2017). As stated earlier, no *MiR338* mutations or variants have yet been identified, so the second criterion is unfulfilled.

Two mechanisms by which miR-338-3p may induce gliomagenesis have been validated thus far, fulfilling the fourth criterion. The first is through de-differentiation, which was reviewed earlier, where miR-338-3p is sufficient to induce differentiation of oligodendrocytes, and loss of miR-338-3p function prevents OPC differentiation into mature oligodendrocytes. The second is inhibition of apoptosis, acting through *MACC1* downregulation (Shang et al., 2016). Like in differentiation, miR-338-3p overexpression in glioma cell lines *in vitro* increased apoptosis and decreased cell viability, but *MACC1* overexpression had the opposite effect, even if miR-338-3p was co-expressed (Shang et al., 2016). The third criterion, *in vivo* confirmation of tumorigenesis in animal models, was confirmed in our laboratory's follow-up sponge experiments (Howe et al., 2017).

In these follow-up experiments, prior students in our laboratory injected the sponge and sensor into the dentate gyrus, and waited 7 days to give the neoplasms time to potentially grow and develop to determine whether these cell clusters were indeed gliomata. Some animals were also administered 5-bromo-2'-deoxyuridine (BrDU) late in incubation and near sacrifice, to examine how these cells proliferated. Following sacrifice, these students stained for nestin, NeuN, GFAP, and BrDU. Nestin and NeuN expression would show whether these clusters were composed of neural precursors or mature neurons, and GFAP expression would reveal whether glia made up the neoplasm, which would indicate that these neoplasms were either gliomata or their precursors.

To the students' surprise, each and every animal treated with miR-338-3p lentiviral knockdown developed regions of neoplasia local to the injection site, composed primarily of cells with miR-338-3p knockdown, expressing both the sponge and the sensor (Fig 6). Nestin expression seemed to be almost entirely localized to the neoplasms' margins, while mostly absent from the neoplasms' center (Fig 6A). GFAP also appeared to be highly expressed at the margins of the neoplastic growths (Fig 6B). The uninfected neurons surrounding the neoplasms expressed NeuN at a much higher rate than in the neoplasms, but they did sporadically observe some NeuN-positive cells within regions of neoplasia (Fig 6C). In observed neoplasms, few cells expressing the miR-338-3p sponge co-expressed BrdU. Instead, they found most BrdU-positive cells on the edge of the neoplasms, with few in histologically normal regions, suggesting the cells on the margins of the neoplasm, adjacent to the sponge-infected cells on the margin, proliferated at an abnormally high rate (Fig 6D). These BrdU-positive cells tended to co-express GFAP as well (Fig 6E). Overall, these neoplasms appeared to consist of a 'core' expressing few biomarkers surrounded by a region of rapidly proliferating nestin- and GFAP-positive cells with small numbers of neurons interspersed throughout the two, consistent with most descriptions of GBM. These data indicated that miR-338-3p loss of function is a direct cause of gliomagenesis *in vivo*.

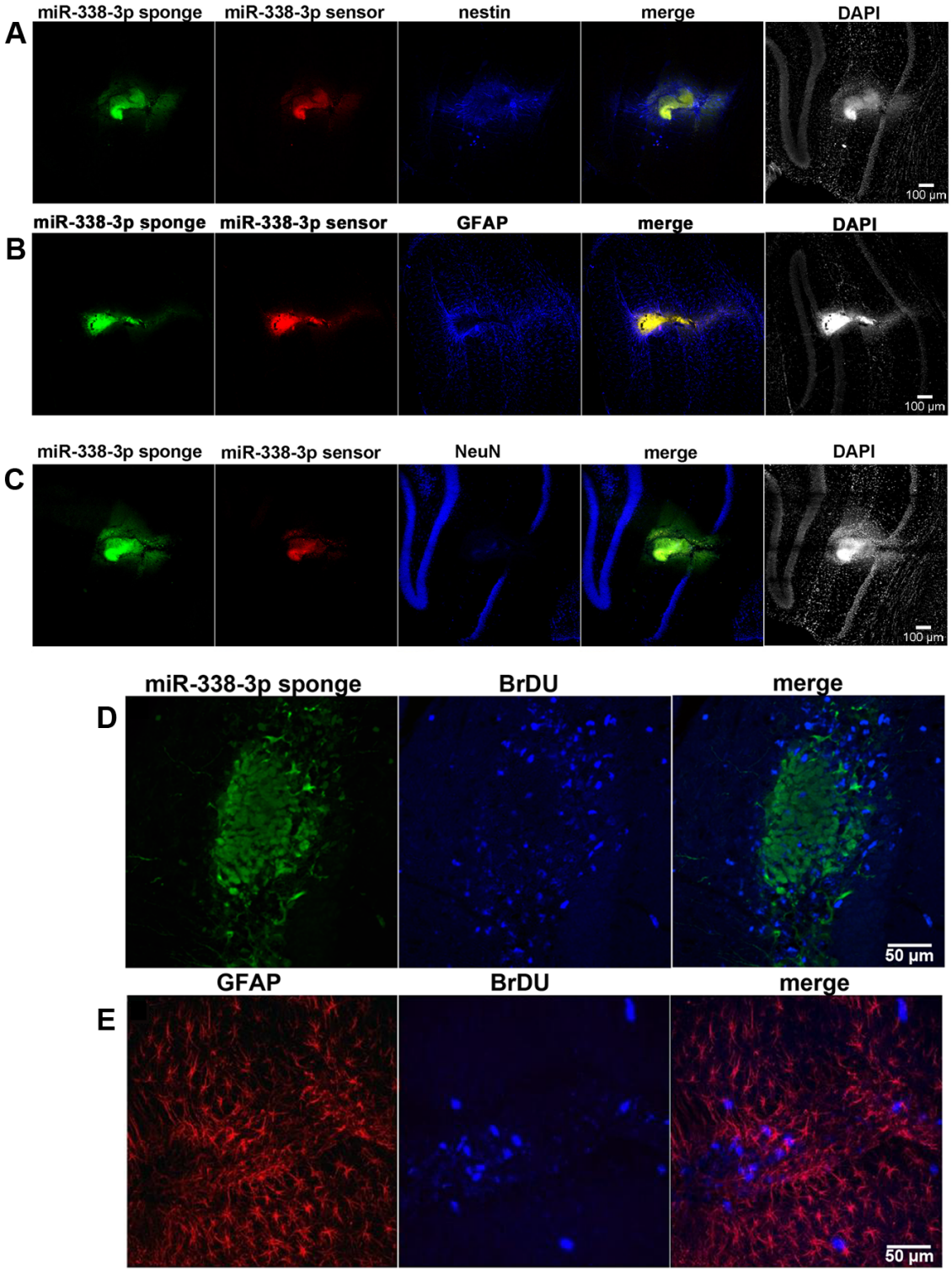

Figure 6. MiR-338-3p knockdown-induced neoplasms histologically resemble GBM. Neoplasms infected with the miR-338-3p sensor (red) and sponge (green) and stained for: **A.** Nestin (blue) as a marker for immature neurons, **B.** GFAP (blue) as a marker for astrocytes, and **C.** NeuN (blue) as a marker for mature neurons. **D.** Expression pattern of of miR-338-3p sponge (green) and BrdU (blue), a marker of cellular proliferation, in a

dentate gyrus neoplasm following miR-338-3p knockdown. **E.** Co-localization of GFAP (red) and BrdU (blue) in dentate gyrus neoplasm following miR-338-3p knockdown. Adapted from (Howe et al., 2017).

Rationale for Current Study

We designed this study to investigate mechanisms by which miR-338-3p acts as a tumor suppressor miRNA in GBM. Earlier studies have characterized low levels of miR-338-3p in GBM biopsies and tumor cell lines, but none have observed direct evidence of loss of miR-338-3p function directly inducing GBM. Prior experiments in our laboratory leading up to this study have characterized miR-338-3p expression patterns in the dentate gyrus, and observed that miR-338-3p knockdown in the dentate gyrus *in vivo* results in neoplasia strongly resembling GBM. Discovering the mechanisms where miR-338-3p may induce GBM in the dentate gyrus would more strongly support the hypothesis that miR-338-3p knockdown in the dentate gyrus directly induces GBM and would fill a large gap where the existing literature is currently sparse. The only mechanistic study of miR-338-3p as a suppressor of GBM only examines apoptosis *in vitro*, and none have yet turned an eye to miR-338-3p's regulation of differentiation or proliferation in GBM. The only investigations of how miR-338-3p regulates cellular development in the nervous system study its effects on oligodendrocytes in the spinal cord and select cortical regions, and none have yet determined its effects on the development of any cells in the hippocampus. This study provides the first description of miR-338-3p's role in the development of cells in the dentate gyrus, and multiple potential mechanistic explanations for miR-338-3p's suppression of GBM not yet found in the literature.

Materials and Methods

Subjects

All procedures were approved by the Institutional Animal Care and Use Committee at the Geisel School of Medicine at Dartmouth College and conformed to federal, state, local, and Association for Assessment and Accreditation of Laboratory Animal Care standards, under Protocol Numbers 11-01-01 and 00002030(a). All mice used were of the C57BL/6J genetic background, obtained from The Jackson Laboratory. Morphology experiments used neonatal mice (postnatal day 7) and GBM graft experiments used adult mice (7-8 weeks of age). All experiments used mixed-sex groups of mice with equivalent numbers of each sex. Animals were housed in a vivarium on a 12-hour light/dark cycle with food and water provided *ad libitum*.

Virus and Vector Design and Production

To generate the miR-338-3p overexpressor virus, the mature miR-338-3p sequence with a canonical stem loop (5'- TTCAAGAGA-3') was cloned into the BbsI/BglII site of pCMVU6, and the U6 promoter and miR338-3p sequence was excised and placed into the PacI/BstB1 site of the lentiviral FUGW vector. Colonies were sequenced to verify that the insert containing target sequences was successfully ligated into FUCW in the desired direction. The miR-338-3p sponge was constructed by inserting 6 perfect miR-338-3p target sequences downstream of the U6 promoter and 6 perfect miR-338-3p target sequences downstream of the H1 promotor via complimentary overhangs to Bbs1/BglII. The sponge cassette was transferred into the retroviral pRubi backbone via ligation into the BstBI and BamHI sites of redRubi. All DNA was collected

using the NucleoBond Xtra Maxi protocol (Macherey-Negel). These viral vectors were designed by Julia Litsky, Emily Li, Patrick Skelton, and Edmond Chipumuro. The pAAV-hSyn-DIO-hM3D(Gq)-mCherry was a gift from Bryan Roth (Addgene plasmid # 44361). The construct is an AAV8 vector, expressing an hM3Dq-mCherry fusion protein under control of the synapsin promoter (Krashes et al., 2011). Meijie Li, a technician in the laboratory, produced all viruses and vectors.

In Vitro Cell Culture

The U251 and SF295 human GBM cell lines and S100β-verbB;Trp53 and GFAP/tTA:TRE/hPDGFB murine cells lines were generously donated by the Israel laboratory at the Geisel School of Medicine at Dartmouth. All cells were cultured in triplicate on 10 cm^3 plates (Corning Incorporated). U251 and SF295 cells were cultured in Dulbecco's Modified Eagle Medium (Life Technologies) containing 10% fetal bovine serum and 1% penicillin/streptomycin. S100β-verbB;Trp53 and GFAP/tTA:TRE/hPDGFB cells were cultured in Iscove's Modified Eagle Medium (ThermoFisher) containing 10% fetal bovine serum, 1% L-glutamine, and 1% penicillin/streptomycin. All cells were incubated in a humidified CO_2 incubator at 37˚C. Prior to infection, the concentration of cells for all cell lines was determined using a hemocytometer, to facilitate numerical precision when plating cells. All cells were visualized for quantification using an Olympus IX-73 fluorescence microscope with a 10x objective lens. All cell lines were infected with viruses at a multiplicity of infection of 20. Following viral infection, all cell lines were incubated for 7 days to ensure full expression of the viral product.

In Vitro Proliferation Analysis

Concentrations of U251 and SF295 cells were quantified daily, and once each plate reached 2×10^5 cells, the cells were infected with either the miR-338-3p overexpressor virus or a control virus expressing only GFP, both within a lentiviral FUGW construct. At 7 days post-infection, the cells were re-plated at 2.5×10^4 cells/plate and counted using a hemocytometer every 24 hours over the course of the next 5 days (8-12 DPI). We were able to perform cell counts for the U251 cells at all time points, but SF295 cells became overconfluent at the time point 96 hours after the beginning of analysis, terminating analysis at 11 days post-infection (DPI). Despite this, growth curves and proliferation rates could be determined from the data for both cell lines.

In Vivo Proliferation Analysis

S100β-verbB;Trp53 and GFAP/tTA:TRE/hPDGFB cells were infected in groups of 1×10^5 cells. Each cell line was divided into 3 groups each, which were subsequently infected with either the miR-338-3p sponge, the miR-338-3p overexpressor, or the control virus expressing GFP, all within a lentiviral FUGW construct, for a total of 6 groups overall. All 6 groups were used in initial GBM model validation experiments and proliferation analyses, while only the GFAP/tTA:TRE/hPDGFB groups infected with the miR-338-3p overexpressor or the GFP-expressing control virus were used in the analysis of neuronal activity's effects on GBM proliferation. In experiments examining neuronal activity in GBM, mice were also injected with either an AAV bearing a construct containing the hM3Dq DREADD or a saline control 21 days before GBM injection

(Smith et al., 2016). For initial GBM validation and proliferation analyses, 5×10^5 cells were injected, and for analyses of neuronal activity on GBM, 1.5×10^5 cells were injected, to compensate for any potential proliferation rate increases resulting from the treatment. All mice were sacrificed at 9 DPI, so they would not be killed by the tumor or display symptoms otherwise requiring sacrifice before the final timepoint (G.J. Rahme, personal communication).

Solution Preparation and Administration

Clozapine-N-oxide (CNO, NIMH Chemical Synthesis and Drug Supply Program) was prepared in a stock solution (2 mM suspended in DMSO) and then diluted in sterile 0.9% sodium chloride solution. Vehicle control was prepared by diluting a proportional amount of DMSO in sterile 0.9% sodium chloride as well. CNO or vehicle was administered twice daily at a dose of 1 mg/kg i.p. following GBM cell injection. CNO or vehicle were administered each day until sacrifice beginning at 1 DPI.

Stereotactic Injections

Mice were anesthetized using an isoflurane gas system (Veterinary Anesthesia Systems Co.) with 4% isofluorane. The mice were secured in a Stoelting lab stereotaxic frame and continued to receive 2% isoflurane through a gas nose cone. To deliver the injectate into the dentate gyrus of adult mice, a one-inch incision was made in the scalp, and holes were drilled through the skull (±1.1 mm lateral, -1.9 mm anteroposterior, -2.5-2.3 mm ventral from bregma). In neonates, incisions were made directly into the skull (±1.3 mm lateral, +1.55 horizontal, -2.3-2.0 mm ventral from lambda). Using a Stoelting

Quintessential Sterotaxic Injector and a 10µl Hamilton syringe, up to 2 µl of injectate was injected into each hemisphere. The syringe was left in place for 2 minutes after injection before being slowly withdrawn. The scalp incision above the injection site was sutured; mice received post-operative topical lidocaine, betadine, and antibiotic ointment at the incision site as well as a peritoneal injection of ketaprofen in saline, then were placed in a recovery chamber until they regained consciousness.

Histology

Mice used for morphological experiments were perfused at 21 DPI, and mice used for graft experiments were perfused at 9 DPI. Mice were deeply anesthetized with 2% avertin, and were transcardially perfused with cold PBS+4% sucrose for approximately 5 minutes, followed by a solution of 4% PFA (paraformaldehyde) in PBS+4% sucrose for approximately 15 minutes. Each brain was post-fixed in 4% PFA in PBS+4% sucrose solution overnight. All sections were cut coronally using a Leica 1200S vibratome. Sections used for morphological analysis were cut 250µm thick. These sections were permeabilized while free-floating for 30 minutes with PBS-T, followed by 2 quick rinses with PBS-T. Sections used for morphological analysis were treated with primary antibodies in PBS with 2% donkey serum and 0.3% Triton X-100 overnight at 4 degrees with chicken anti-GFP (1:2000, Abcam) and rabbit anti-mCherry (1:2000, Abcam) primary antibodies. The following day, sections were washed 3 times every 15 minutes, followed by 2 quick rinses with PBS-T. Primary antibodies were detected using the Alexa488 anti-chicken and Cy3 anti-rabbit secondary antibodies (1:200, Jackson Immunoresearch). These sections were incubated overnight before mounting. Sections

from graft experiments were cut 50µm thick. These sections were not stained, using endogenous fluorescence for imaging. All sections were permeabilized by PBS-T immediately prior to mounting on glass cover slips with VectaShield Antifade Mounting Medium with DAPI (Vector Labs).

Image Analysis

Sections for morphology analysis were imaged using a Zeiss LSM 510 confocal microscope. Morphological sections were imaged using a 20x oil lens with 3x digital zoom and analyzed over an area of 225 μm^2 at the maximum possible depth. Between one to four images were quantified per injected mouse. To analyze differences in the morphology of dendritic spines, a 63x oil lens with 3x digital zoom was used to take images of dendrite segments of neurons immunostained with Alexa488 or Cy3. Point-spread functions (PSFs) were generated for the image using the PSF Generator plugin for ImageJ, and then images were deconvolved using a Richardson-Lucy function based in the DeconvolutionLab plugin for ImageJ. The NeuronStudio program (Mount Sinai School of Medicine Computational Neurobiology and Imaging Center) was then used to automatically quantify deconvolved segments of dendrites for spine density, spine length, and spine head diameter. Tumor volume was estimated in NeuroLucida using a 3D reconstruction protocol described previously (Fricano-Kugler et al., 2016).

Statistical Analysis

For the *in vitro* proliferation assays, we performed repeated-measures two-way ANOVA analyses in Stata 13.1.206 (StataCorp LP). For each morphological analysis, we

performed a t-test, Kolmogorov-Smirnov test, or ANOVA analyzed post-hoc via Tukey's range test in Stata 13.1.206. We accounted for individual differences in counts and measurements of neurons between mice using previously described models (Moen et al., 2016). Significance was set at $p<0.05$ for all analyses. All figures were created using GraphPad Prism 6 (GraphPad Software, Inc.).

Results

MiR-338-3p Knockdown Contributes To Aberrant Granule Neuron Morphology

To determine the mechanism by which miR-338-3p loss contributes to GBM, we began by examining the effects of miR-338-3p knockdown on the development of granule neurons in the dentate gyrus. Granule neurons in the dentate gyrus display a very fixed and well-characterized morphology in an easily visible and highly specific location. Granule neurons allow for much more robust quantifications of many aspects of their morphology compared to other local cell types, because a greater number of stable morphological characteristics can be quantified and aberrant development can be easily identified, which is especially important *in vivo*. Dentate gyrus neural stem cells that give rise to granule neurons throughout neurogenesis additionally give rise to oligodendrocytes and astrocytes. This leaves open the possibility that any morphometric differences observed resulting from miR-338-3p's knockdown throughout development may be relevant to oligodendrocytes and astrocytes, which could be pursued in future lines of research. We chose a knockdown strategy because it applies the same manipulation that induced neoplasia in prior experiments, maximizing the relevance of the potential observed changes to the original neoplasia induced by miR-338-3p knockdown.

To knock down miR-338-3p *in vivo*, we used the sponge construct designed and characterized by Emily Li, a prior undergraduate in the laboratory (refer back to Figure 5 for construct design). The construct was originally expressed in a lentiviral FUGW vector, which infected neurons at all stages of maturity. To ensure the sponge construct was expressed throughout all infected neuron's development, we cloned the construct

into a retrovirus using the pRubi vector backbone, limiting infection to actively proliferating neural stem cells in the dentate gyrus. This allows examination of miR-338-3p's effects on the development of granule neurons exclusively in those neurons experiencing miR-338-3p knockdown through its entire development. We co-injected the sponge retrovirus in equal proportion with a control retrovirus bearing a similar pRubi construct expressing only GFP, comparing granule neurons that developed under miR-338-3p-deficient conditions with granule neurons that developed under wild-type conditions.

21 days after infection, both constructs had highly infected the granule cell layer of the dentate gyrus. The majority of labeled cells were infected by the sponge vector alone or co-infected by the control and sponge vectors (co-expressing mCherry and GFP, phenotypically similar to neurons infected with the sponge construct), and only a minority was infected solely with the GFP control vector (Figure 7A). Both of the constructs provided sufficient resolution for visualization of labeled cells to perform analysis at the levels of both the whole neuron and the single dendritic spine (Figure 7A-B). We limited our morphological analysis to granule neurons, which made up the majority of infected cells, but other cell types were infected as well. We could observe regions of neoplasia in multiple animals near sites local to those chosen for quantification of identified infected neurons.

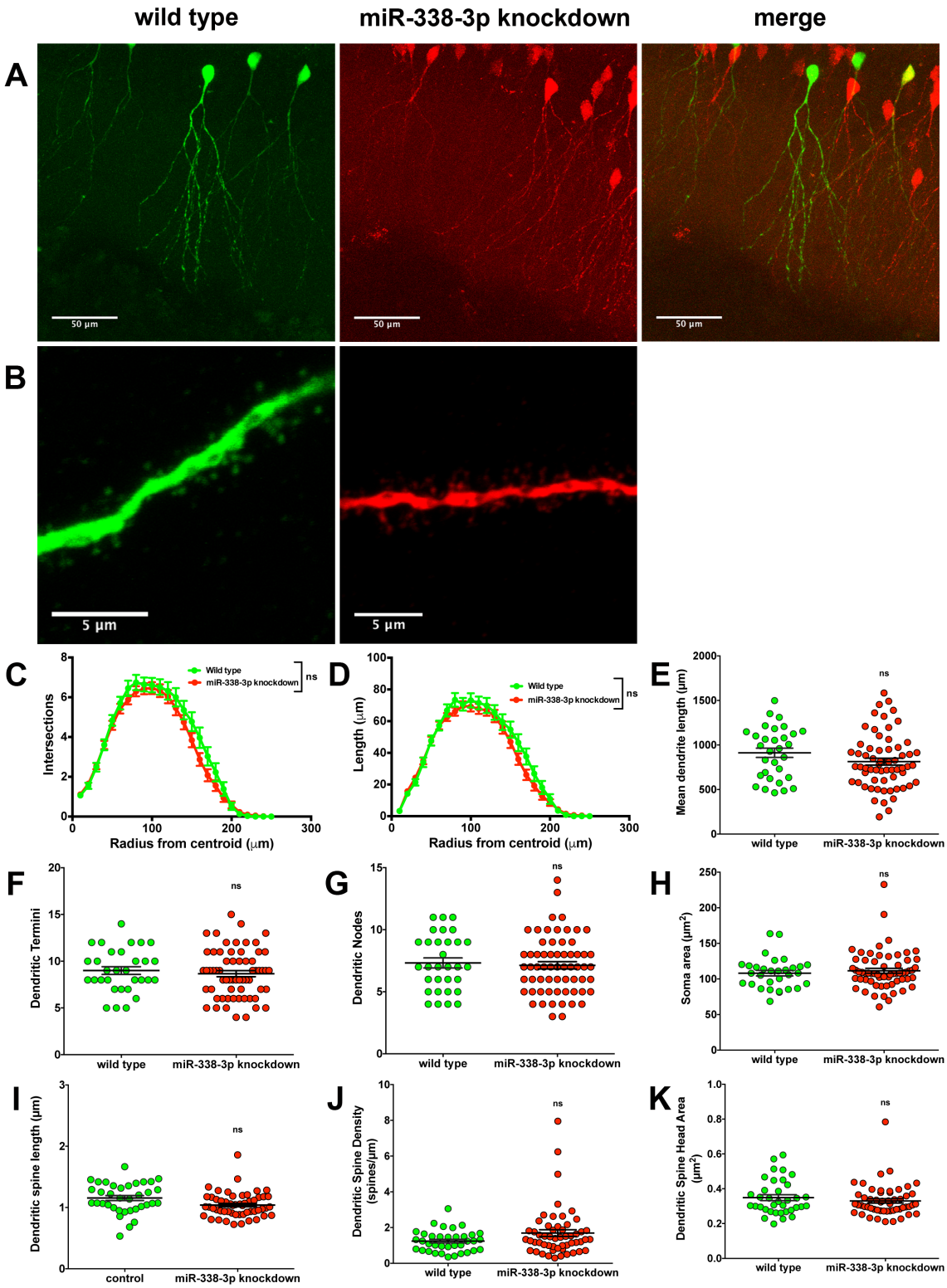

Figure 7. Representative images of granule neuron morphology and unaltered morphometric characteristics following miR-338-3p knockdown. Retroviruses expressing either a sponge to knock down miR-338-3p expression or GFP as a control were co-injected into the dentate gyrus of 8-week old young adult mice to determine the

role of miR-338-3p in the morphological development of newborn granule neurons. **A.** Representative images of granule neurons expressing GFP and/or the miR-338-3p sponge construct at moderate magnification. The miR-338-3p sponge construct infected granule neurons at a higher rate than the GFP construct. **B.** Representative images of granule neuron dendrites and dendritic spines at high magnification infected with the GFP control construct or the miR-338-3p sponge construct . **C.** Sholl analysis of intersections. No overall significant difference in dendritic branching as measured by amount of intersections with shells at regular distances from the center of the soma was detected between the wild type (n=31 neurons, 5 animals) and miR-338-3p knockdown (n=63 neurons, 5 animals) conditions (Kolmorogov-Smirnov test D=0.16, p>0.05). **D.** Sholl analysis of length. No overall significant difference in dendritic length between shells at regular distances from the center of the soma was detected between the wild type (n=31 neurons, 5 animals) and miR-338-3p knockdown (n=63 neurons, 5 animals) conditions (Kolmorogov-Smirnov test, D=0.20, p>0.05). **E.** Mean lengths of primary dendrites. No significant difference in mean length of primary dendrites was observed between the wild type (n=31 neurons, 5 animals) and miR-338-3p knockdown (n=63 neurons, 5 animals) conditions (unpaired t-test, t_{92}=1.51, p>0.05). **F.** Amounts of dendrite endings per neuron. No significant difference in number of dendrite endings per neuron was observed between the wild type (n=31 neurons, 5 animals) and miR-338-3p knockdown (n=63 neurons, 5 animals) conditions (unpaired t-test, t_{92}=0.613, p>0.05). **G.** Amounts of dendrite branch nodes per neuron. No significant difference in number of dendrite branch nodes per neuron was observed between the wild type (n=31 neurons, 5 animals) and miR-338-3p knockdown (n=63 neurons, 5 animals) conditions (unpaired t-test, t_{92}=0.386, p>0.05). **H.** Soma surface area. No significant difference in soma surface area was observed between the wild type (n=31 neurons, 5 animals) and miR-338-3p knockdown (n=63 neurons, 5 animals) conditions (unpaired t-test, t_{92}=0.617, p>0.05). **I.** Dendritic spine length. No significant difference in dendritic spine length was observed between the wild type (n=36 dendrites, 5 animals) and miR-338-3p knockdown (n=54 dendrites, 5 animals) conditions (unpaired t-test, t_{88}=1.310, p>0.05) **J.** Dendritic spine density. No significant difference in dendritic spine density was observed between the wild type (n=36 dendrites, 5 animals) and miR-338-3p knockdown (n=54 dendrites, 5 animals) conditions (unpaired t-test, t_{88}=1.861, p>0.05). **K.** Dendritic spine head area. No significant difference in dendritic spine head area was observed between the wild type (n=36 dendrites, 5 animals) and miR-338-3p knockdown (n=54 dendrites, 5 animals) conditions (unpaired t-test, t_{88}=0.931, p>0.05). ns p>0.05. All results show mean ± SEM.

Sholl analyses of intersections and length showed miR-338-3p knockdown during granule neuron development does not induce significant changes in number of shell intersections or dendrite length between shells at any distance from the soma (p>0.05, Figure 7C-D). Similarly, we did not observe any statistically significant changes in soma surface area, number of dendrite branch nodes, number of dendrite endings, and mean

primary dendrite length following miR-338-3p knockdown over the course of neuronal development (Figure 7E-H, $p>0.05$). We did not find statistically significant changes in any property of dendritic spines, including dendritic spine density, length, or head area at neuronal maturity under miR-338-3p knockdown conditions (Figure 7I-K, $p>0.05$). In short, miR-338-3p has no significant effect on most aspects of dendritic morphology in the dentate gyrus, including dendritic arborization, soma size, and dendritic spines.

However, miR-338-3p did exert some highly specific effects on the development of granule neuron morphology. The granule neurons expressing the miR-338-3p sponge tended to display abnormal proximal dendritic architecture, where dendrites protruded from the soma at abnormal angles (Figure 8A). The granule cell is a bipolar neuron, projecting a single primary dendrite into the molecular layer oriented orthogonal to the hilus/granule cell border. To quantify the change in somatodendritic sprouting caused by miR-338-3p knockdown, we traced a line 90˚ from the granule layer/hilus border to the center of the soma, followed by a second line along the axis of the dendrite, and then we measured the angle between the cell body and dendrite (Figure 8A). The granule cells expressing only the control vector had a mean branch angle of 163.9 ± 2.2˚, while the granule cells expressing the miR-338-3p sponge had a mean branch angle 155.8 ± 1.7˚, with a mean difference in branch angle of 8.0 ± 2.8˚. This magnitude of this difference indicated significant deviation from the wild type mean branch angle in miR-338-3p knockdown neurons (Fig. 8C; t_{88}=-2.27, $p<0.05$).

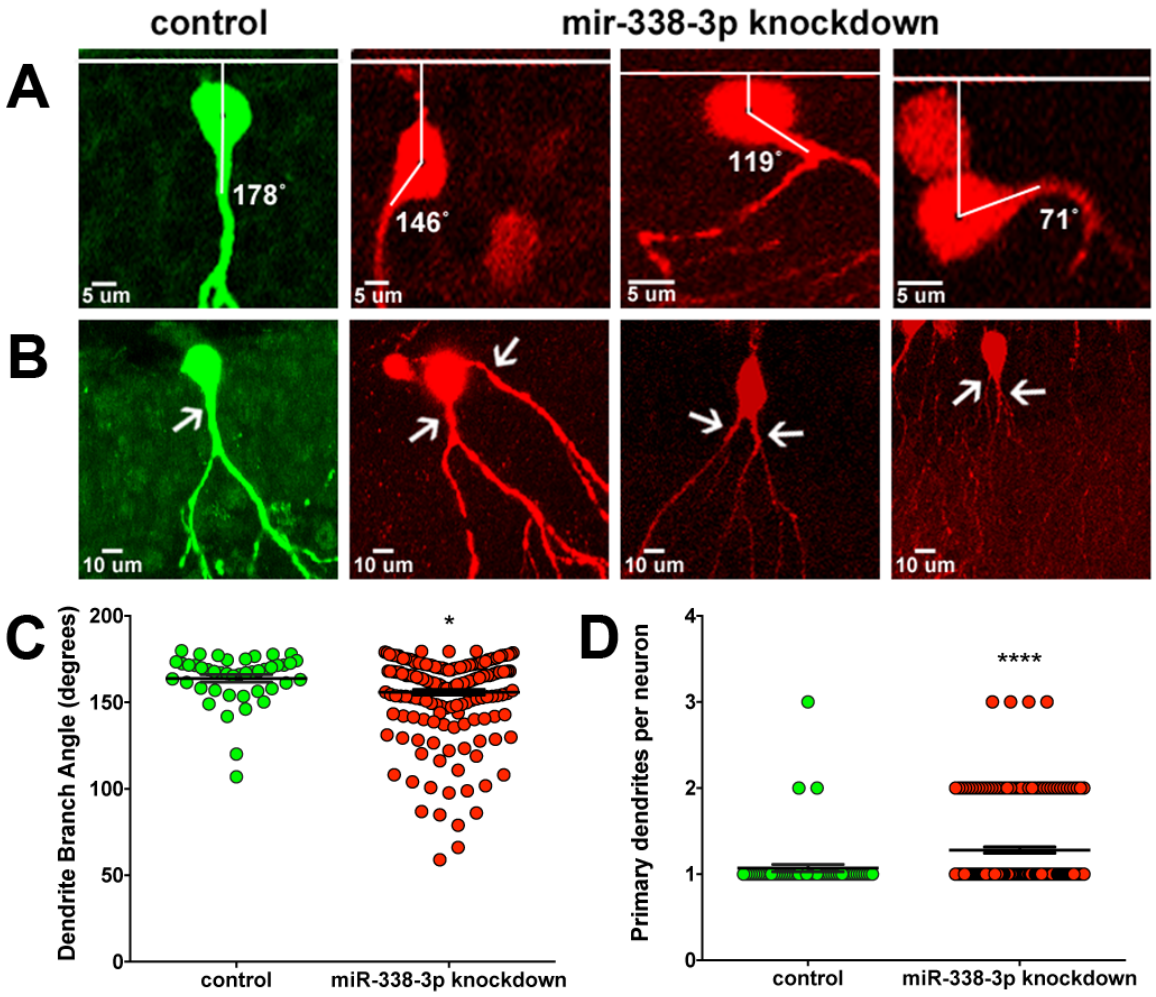

Figure 8. MiR-338-3p knockdown gives rise to aberrant morphological characteristics in infected granule neurons. At 21 DPI, granule neurons infected with the knockdown sponge construct displayed specific morphological changes not generally present in granule neurons infected with the control GFP construct. **A.** Representative images highlighting somatodendritic branching in GFP-expressing wild type granule neurons and mCherry-expressing granule neurons where miR-338-3p is knocked down. **B.** Representative images highlighting amount of primary dendrites in GFP-expressing wild type granule neurons and mCherry-expressing miR-338-3p knockdown granule neurons. **C.** Branch angles of primary dendrites infected with either the GFP control construct or the miR-338-3p knockdown construct. Knockdown of miR-338-3p throughout granule neuron development significantly reduces the branch angle of primary dendrites relative to the border between the hilus and granule cell layer ($p<0.05$). **D.** Number of primary dendrites in granule neurons infected with either the GFP control or the miR-338-3p knockdown construct. Knockdown of miR-338-3p throughout granule neuron development significantly increases the mean amount of primary dendrites per granule neuron. *$p<0.05$, ****$p<0.0001$. Unpaired t-test. Control n=31 neurons, 5 animals; Knockdown n=63 neurons, 5 animals. All results show mean ± SEM.

Many of the visible granule cells appeared to sprout multiple primary dendrites (Fig 8B). In neurons expressing the miR-338-3p sponge, there were 1.28 ± 0.04 primary dendrites/neuron on average, while control neurons averaged 1.07 ± .04 primary dendrites/neuron, resulting in a significant increase in the number of primary dendrites/neuron in miR-338-3p-deficient cells (Fig 8D; t_{88}=4.57, p<0.0001). These data indicate miR-338-3p knockdown does bias granule neurons toward sprouting multiple primary dendrites. The majority of neurons with multiple primary dendrites had two and a minority had three, but none had four or more. When neurons expressed the aberrant phenotype, the primary dendrites organized in one of two arrangements: one primary dendrite in the correct apical orientation and another basal dendrite branching off at an angle approximately perpendicular to the other (Fig 8B, second image), or both sprouting apically at angles close to the wild-type orientation, diverging away from the soma in opposing directions (Fig 8B, third and fourth image).

Taken together, these morphological changes indicate aberrant primary dendrite organization in granule neurons that develop under conditions of low miR-338-3p expression. However, despite the wide range of genes regulated by miR-338-3p, these morphological changes are limited to the manner by which the primary dendrite sprouts off of the soma, inducing no other significant morphological changes at all other levels of granule neuron organization.

MiR-338-3p Inhibits GBM Cell Proliferation *In Vitro*

The first portion of this study examined how miR-338-3p leads to GBM by determining its impacts on neuronal development, only one of three mechanisms. The

next part of our study investigates miR-338-3p's effect on proliferation, the final unstudied core mechanism by which miR-338-3p may induce gliomagenesis. We initially assayed proliferation *in vitro* because it is much easier and reliable than *in vivo*, allowing greater sensitivity to putative effects, despite the loss of experimental construct validity.

We chose the human GBM cell lines U251 and SF295 as an *in vitro* model of GBM to model the impact of miR-338-3p on GBM proliferation. We chose these two cell lines because neither cell line expresses miR-338-3p at detectable levels, allowing them to model GBM expressing miR-338-3p at low levels (Gaur et al., 2007). We assayed two cell lines to ensure that any effect of miR-338-3p on proliferation did not result from a property of the cell line unrelated to GBM and that any observed effect would likely generalize across GBM instead of applying to just a single cell line.

To determine the effect of miR-338-3p on the proliferation of GBM cells expressing the miRNA at low levels, we used an overexpression construct to restore miR-338-3p expression. The overexpression construct expressed a GFP reporter under the control of a constitutive ubiquitin promoter, and two mature miR-338-3p sequences under control of the U6 promoter, a strong promoter of siRNA expression, to express the miRNA in these miR-338-3p-deficient GBM cells (Figure 9A).

We validated the overexpressor's function by co-infecting the two cell lines with the miR-338-3p sensor and a construct containing either the miR-338-3p overexpressor or the GFP reporter alone (Figs 9B-E). We noted a clear decrease in expression of the mCherry sensor in both cell lines when infected with the overexpression construct, indicating an increase in miR-338-3p expression in infected cells. From this, we could conclude the overexpressor effectively induced miR-338-3p expression in both cell lines.

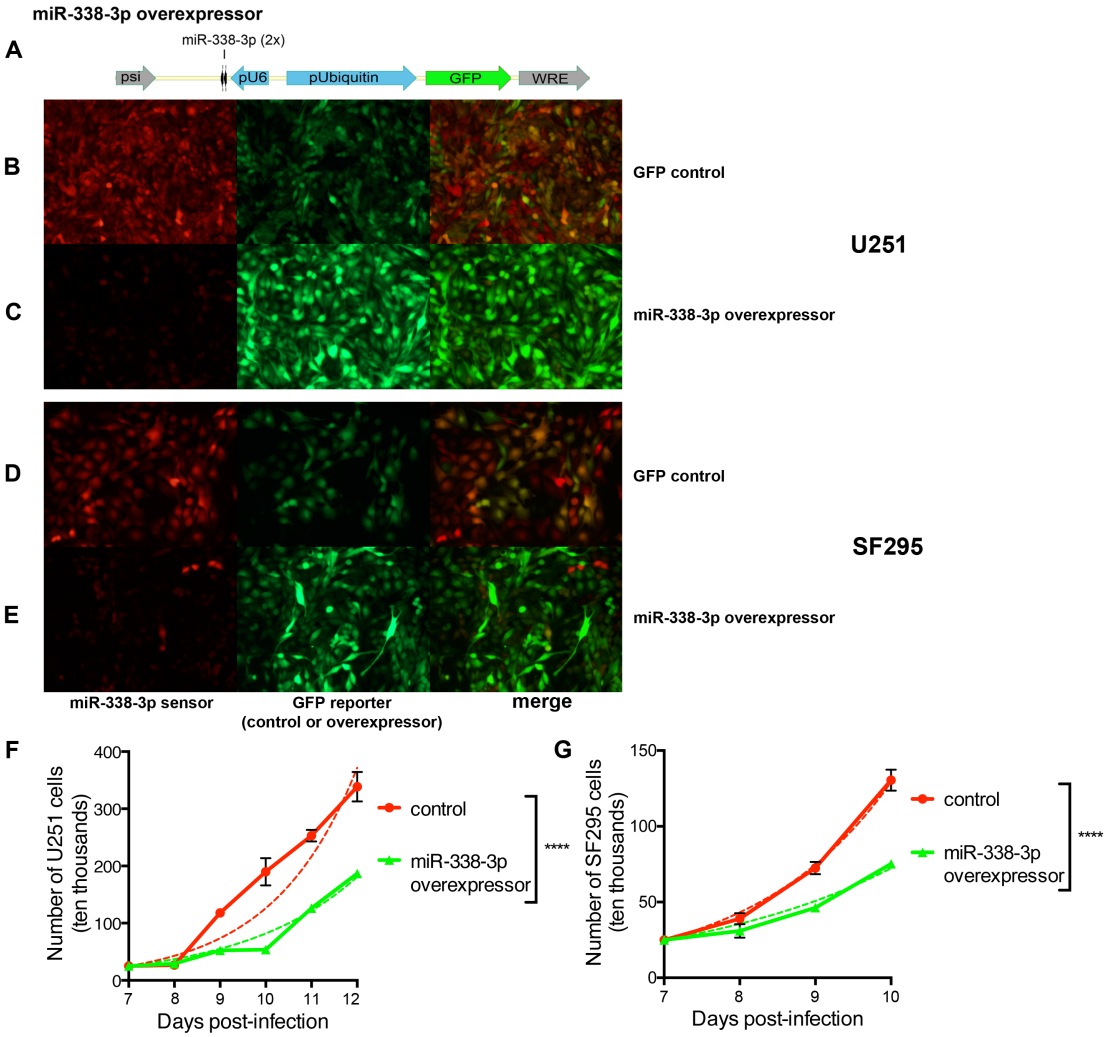

Figure 9. Overexpression of miR-338-3p inhibits proliferation of two miR-338-3p-deficient GBM cell lines *in vitro*. A. MiR-338-3p overexpression construct design. Cells infected with the construct constitutively express GFP as a reporter under the control of the ubiquitin promoter and two mature miR-338-3p transcripts under the control of the U6 siRNA promoter. **B.** Endogenous miR-338-3p expression in U251 GBM cells. Cells were infected with the mCherry (see Figure 3 for design) miR-338-3p sensor construct and a control construct expressing GFP. High mCherry expression compared to GFP confirms very low miR-338-3p expression in U251 cells. **C.** Expression of mCherry miR-338-3p sensor following infection with the overexpressor construct. High GFP and low mCherry expression indicates successful overexpressor infection and overexpression of miR-338-3p in U251 cells, respectively. **D.** Endogenous miR-338-3p expression in SF295 GBM cells. These cells were infected with the mCherry-expressing miR-338-3p sensor construct and a control construct expressing GFP. High mCherry expression compared to GFP confirms very low miR-338-3p expression in SF295 cells. **E.** Expression of mCherry miR-338-3p sensor following infection with the overexpressor construct in SF295 cells. High GFP and low mCherry expression indicates successful overexpressor infection and overexpression of miR-338-3p in SF295 cells, respectively.

F. Population growth kinetics of U251 GBM cells infected with either an empty vector or miR-338-3p overexpressor construct from 7-12 DPI. Overexpression of miR-338-3p significantly reduces *in vitro* proliferation of U251 cells ($p<0.001$). **G.** Population growth kinetics of SF295 GBM cells infected with either an empty vector or miR-338-3p overexpressor construct from 7-12 DPI. Overexpression of miR-338-3p significantly reduces *in vitro* proliferation of SF295 cells ($p<0.001$). Dotted lines fit theoretical population growth curves to the observed data, using the equation: $Y = 25 \times 2^{t/DT}$, where Y is the number of cells at time t and DT is the doubling time. ****$p<0.001$. Repeated-measures two-way ANOVA. All measurements were performed in triplicate at all time points in all groups. Results show mean ± SEM.

To investigate the impact of miR-338-3p on cellular proliferation, we examined population growth kinetics for the U251 and SF295 cell lines infected with the miR-338-3p overexpressor. In both cell lines, miR-338-3p overexpression decreased the proliferation rate compared to control (Figs 7F and 7G). The control population was approximately double that of the miR-338-3p overexpressing population at the final time point in both cell lines. In U251 cells, there were $34.1 \pm 4.95 \times 10^5$ cells in the control population and $18.7 \pm 1.55 \times 10^5$ cells in the miR-338-3p-overexpressing population at 12 DPI, with corresponding doubling times of 16.9 and 19.3 hours respectively, indicating an significant overall reduction in proliferation rate (Fig 7F; $F_{1,6}$=69.32, $p<0.0001$). Overexpression in SF295 cells yielded similar results: $13.05 \pm 1.38 \times 10^5$ control cells and $7.525 \pm 0.275 \times 10^5$ miR-338-3p overexpressing cells were present at 10 DPI, with respective doubling times of 12.6 and 14.7 hours (Fig 7G; $F_{1,6}$=53.19, $p<0.0001$). These results indicate miR-338-3p inhibits GBM proliferation *in vitro*.

Development of an *In Vivo* GBM Model

In the previous section of the study, we showed miR-338-3p inhibits proliferation of multiple GBM cell lines *in vitro.* However, *in vitro* studies cannot fully describe the true effect of miR-338-3p on GBM, because the *in vitro* environment does not fully

recapitulate the conditions the tumor exists within that may be crucial to its proliferation, such as microenvironment, immune response, and adjacent cells, among others. Recapitulating the effect *in vivo* is a crucial step to ensure the effect is truly consequential. To this end, we developed an *in vivo* cancer cell line graft model of GBM in the dentate gyrus. We introduced GBM into the dentate gyrus via direct implantation, injecting GBM cells into the murine dorsal dentate gyrus.

We modeled GBM using two separate murine cancer cell lines, both derived from primary tumors arising from a transgenic mice designed to develop glioblastoma (referred to by the their transgenic strain of origin). The first cell line was derived from a primary high-grade glioma arising from the spinal cord of a GFAP/tTA:TRA/hPDGFB transgenic mouse on a C57BL/6J genetic background (Hitoshi et al., 2008). The second cell line was derived from a primary high-grade glioma within the subventricular zone of an S100β-verbB;Trp53 mouse, also on a C57BL/6J background (Harris et al., 2008). Implantation of these two cell lines into wild-type C57BL/6J mice is an allograft, where tissue from a donor is grafted into a sufficiently syngeneic (i.e. same mouse strain) recipient. Allograft models are advantageous because grafted syngeneic cells do not provoke an immune response in the recipient, unlike xenograft models, which require immunosuppressed nude mice, greatly reducing construct validity (Teicher, 2006).

We infected both of these cell lines with either a reporter vector expressing only GFP, the lentiviral miR-338-3p overexpressor, or the lentiviral miR-338-3p sponge. We incubated the infected GBM cells for 7 days, and then allografted them into the dorsal dentate gyrus of adult C57BL/6 mice. Following a 9-day incubation *in vivo*, we harvested the tumors, sectioned them, and looked for GFP (to identify GBM cells) and DAPI (a

nuclear stain to reveal gross anatomical context), then reconstructed using 3-dimensional alignment and analyzed by estimating the volume of tissue expressing GFP.

In the GFAP/tTA:TRA/hPDGFB allografted GBM cells, we witnessed strong GFP fluorescence regardless of the vector the cells were infected with prior to implantation (Figure 10A, 10B). Most GFAP/tTA:TRA/hPDGFB GBM cells expressed GFP at a high level, though small patches within the tumor display reduced GFP expression compared to their surrounding cells (Figure 10A, left and right columns). DAPI fluorescence suggests these patches are histologically similar to the rest of the tumor. All individuals in all groups allografted with GFAP/tTA:TRA/hPDGFB developed tumors expressing GFP at the proper location, with the needle track terminating in the superior dorsal dentate gyrus, near the crest and suprapyramidal blade.

GBM cells were found descending down the needle track, forming a column traveling up from the main GBM mass, through the cortex and up to the injection site at its surface (Figure 10A, middle column). However, the GBM is not centered on the needle track and forms an asymmetric oblong shape (Figure 10B, 10C). GBM growth is biased caudally, with the needle track positioned at the extreme rostral end of the GBM. The GBM then grows through the entirety of the dorsal hippocampus caudal to the needle track (Figure 10A, left column). As the dorsal hippocampus laterally transitions to the ventral hippocampus when becoming more caudal, the GBM continues to grow in the same direction, gradually growing medial to the ventral hippocampus, invading into the subiculum (Figure 10A, right column). Overall, dentate gyrus allograft of GFP-expressing GFAP/tTA:TRA/hPDGFB cells reliably models hippocampal GBM, displaying consistently high tumor visibility and a robust morphology across groups.

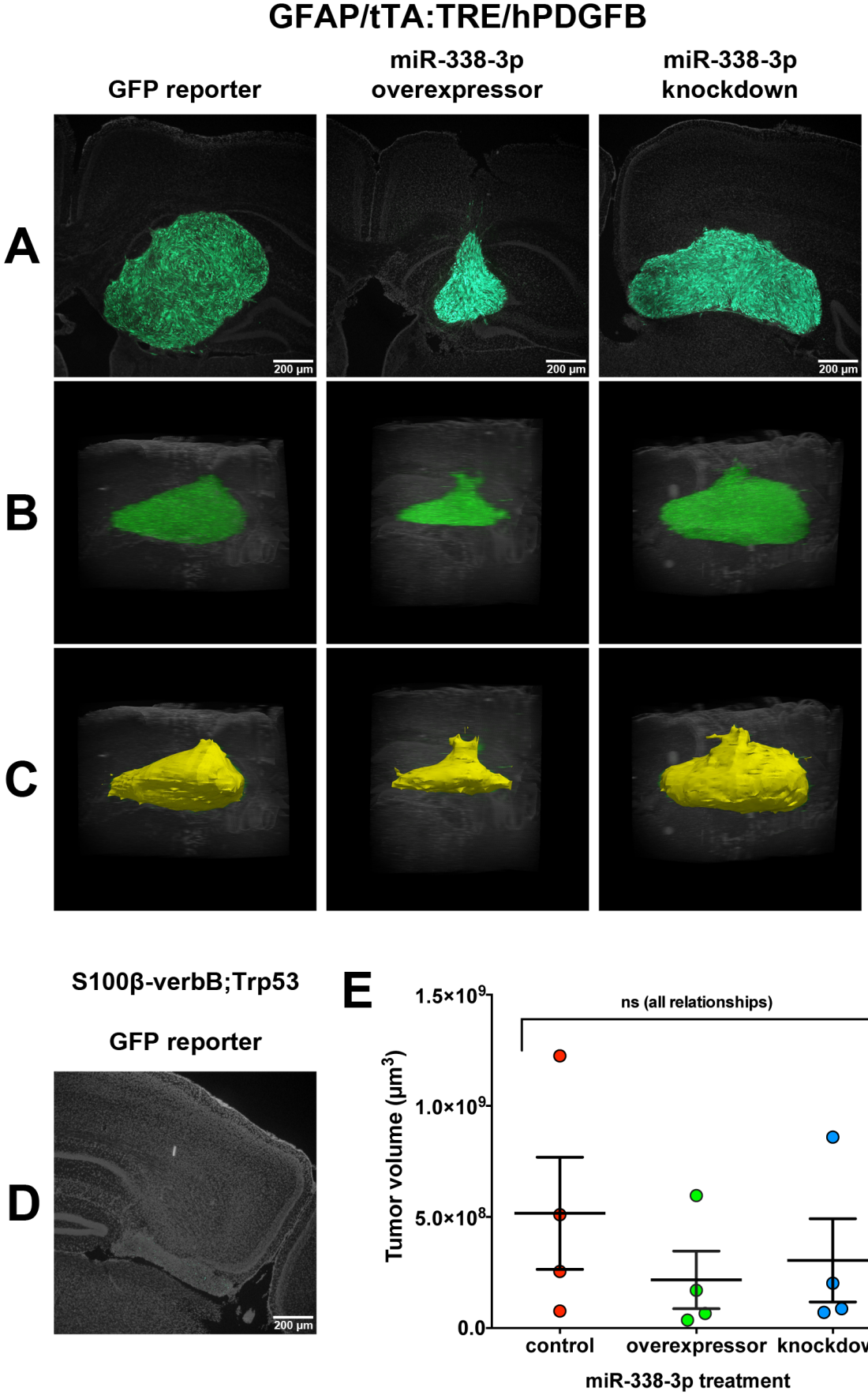
GFAP/tTA:TRE/hPDGFB
GFP reporter
miR-338-3p overexpressor
miR-338-3p knockdown
A
B
C
200 µm
S100β-verbB;Trp53
GFP reporter
D
E
1.5×10^9
1.0×10^9
5.0×10^8
0.0
Tumor volume (µm^3)
ns (all relationships)
control
overexpressor
knockdown
miR-338-3p treatment

Figure 10. MiR-338-3p has no detectable effect on GBM proliferation in an *in vivo* allograft model of hippocampal GBM. A. Representative images of coronal cross-sections of brains stained with DAPI (grey) and injected with GFAP/tTA:TRA/hPDGFB GBM cells infected with either a GFP reporter (left), miR-338-3p overexpressor (middle), or miR-338-3p sponge. Representative cross-sections taken from three distinct segments of the tumor, from left to right: segment within hippocampus, injection site, and segment invading subiculum. **B.** 3D models of GBM created from aligned coronal serial cross-sections of xenografted GBM expressing GFP (green) and the surrounding tissue expressing DAPI (grey), containing the cross-sections from Figure 10A. **C.** 3D reconstructions of the allografted GBM (yellow) from closed contour tracings of 3D models in Figure 10B. **D.** Representative image of S100β-verbB;Trp53 GBM cells expressing only GFP (green) transplanted into the murine hippocampus. Few cells express GFP and those express GFP do so at low levels. Transplanted cells are only visible as a cluster of DAPI (grey) signal not corresponding to known gross anatomy of the hippocampus and adjacent cortex in the general region where GFAP/tTA:TRA/hPDGFB GBM cells invaded. Transplanted S100β-verbB;Trp53 GBM cells infected with the miR-338-3p overexpressor or sponge expressed similarly low levels of GFP. **E.** Mean volumes of tumors resulting from orthotopic allografts of GFAP/tTA:TRA/hPDGFB GBM cells into the murine hippocampus, previously infected with a GFP reporter, the miR-338-3p overexpressor, or the miR-338-3p sponge. Alterations to miR-338-3p expression in either direction had no significant effect on the volume of the resulting tumor ($p>0.05$ overall, all individual comparisons). ns $p>0.05$. One-way ANOVA with multiple comparisons. n=4, all groups. Results show mean ± SEM.

Conversely, the injected S100β-verbB;Trp53 cells modeled GBM poorly. The cells expressed GFP at a very low level, to the point where only a few cells displayed visible fluorescence, preventing us from performing accurate or precise volume estimations (Figure 10D). We could observe GBM at very low resolution, because visible clusters of cells not corresponding to any known gross anatomy of the hippocampal formation arose in approximately the same location as the GFAP/tTA:TRA/hPDGFB GBM. We could not reliably demarcate the exact dimensions of the putative tumor due to lack of GFP expression, but the cluster of S100β-verbB;Trp53 GBM cells did not appear to thrive to the same degree as the GFAP/tTA:TRA/hPDGFB GBM cells; their morphology seemed much more constrained by the surrounding tissue, and despite our inability to quantify its volume, the cluster of S100β-verbB;Trp53 cells in serial sections

detected via DAPI appeared visibly smaller than corresponding sections from GFAP/tTA:TRA/hPDGFB GBM. As a result of our inability to quantify the volume of GBM arising from S100β-verbB;Trp53 cells and these cells' failure to thrive upon implantation, we decided not to use S100β-verbB;Trp53 cells for further modeling of GBM *in vivo.* Due to unsuitability of this cell line for volume analysis, we performed all further *in vivo* GBM modeling and analysis using the GFAP/tTA:TRA/hPDGFB GBM cell line exclusively.

To investigate the impact of miR-338-3p expression on tumor proliferation *in vivo,* we analyzed the differences in tumor volume between the groups infected with the three different vectors inducing differential miR-338-3p expression (Figure 10E). GBM expressing the GFP reporter virus had a mean volume of $5.17 \pm 2.17 \times 10^8$ μm^3, while the mean volume of GBM expressing the miR-338-3p overexpressor was $2.17 \pm 1.30 \times 10^8$ μm^3 and the mean volume of GBM expressing the miR-338-3p sponge was $3.05 \pm 1.87 \times 10^8$ μm^3. Overall, the level of miR-338-3p expression between the three groups did not significantly alter GBM volume (Figure 10E; $F_{2,9}=0.617$, $p>0.05$).

However, the means of the different groups were relatively distinct from one another, while the variance within each group was disproportionately high. To determine whether the results are likely due to lack of a true effect or due to low statistical power, we conducted a post-hoc power analysis. The power of this analysis was .183, which both indicates the test was very underpowered and reveals a Type II error probability of .817. *Ceteris paribis,* increasing the sample size of all groups to 7 subjects each would be sufficient to detect a significant effect in this analysis, according to our power analysis.

The Effect of Neuronal Activity on GBM Proliferation *In Vivo*

Recently, a high-profile study reported results suggesting that increases in local neuronal activity increase glioma proliferation (Venkatesh et al., 2015). Their findings are provocative because epilepsy is a common symptom of glioma, partially due glutamate secretion by gliomata themselves (Buckingham et al., 2011). Such an effect would suggest that epilepsy directly causes tumor progression, instead of solely functioning as a symptom associated with glioma progression. Their results potentially shed light on the influence of the *in vivo* microenvironment on GBM proliferation.

We attempted to replicate their findings using our newly developed allograft GFAP/tTA:TRA/hPDGFB *in vivo* hippocampal GBM model. While their study used optogenetics to induce neuronal activity, we used a designer receptor exclusively activated by designer drug (DREADD) system, specifically the hM3Dq-mCherry receptor, which is a mutated muscarinic M3 receptor activated by CNO and coupled to the G_q pathway, which induces neuronal burst firing akin to *status epilepticus*, fused with mCherry as a reporter (Alexander et al., 2009). We segregated mice into four groups, with two as controls: one group administered CNO but given a sham surgery and one administered a vehicle but infected with the virus bearing the hM3Dq-mCherry construct, to ensure neither had an effect on their own. The third group had the entire DREADD system (administered CNO and expressed the hM3Dq) and all three of these groups were injected with GBM cells expressing the GFP reporter. The fourth group carried the DREADD system, but we injected them with GBM cells expressing the miR-338-3p overexpressor to determine if miR-338-3p overexpression could potentially mitigate proliferation increases in glioma induced by the DREADD.

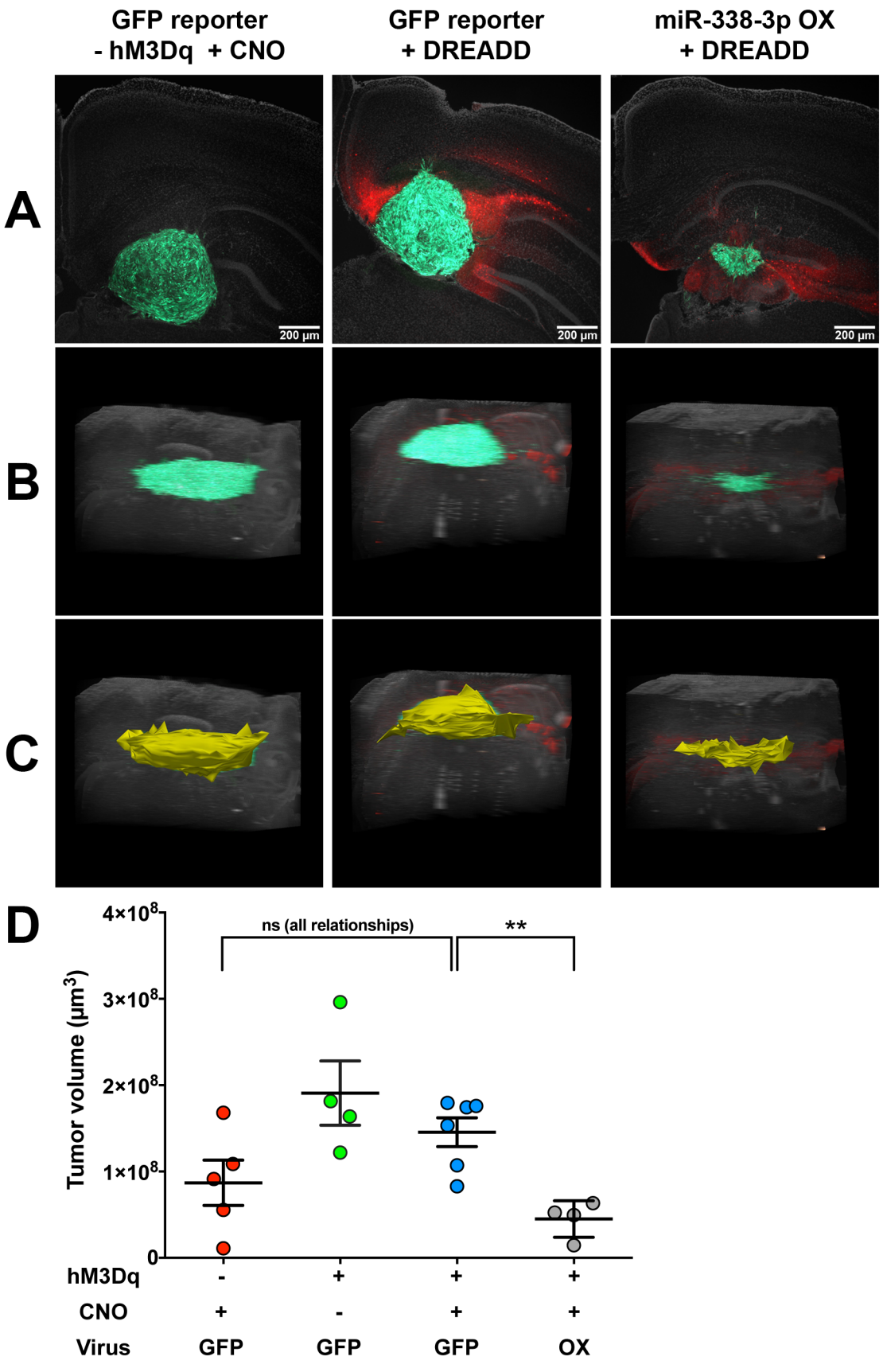
GFP reporter
- hM3Dq + CNO
GFP reporter
+ DREADD
miR-338-3p OX
+ DREADD
A
B
C
D
200 µm
200 µm
200 µm
ns (all relationships)
**
Tumor volume (µm3)
4×10^8
3×10^8
2×10^8
1×10^8
0
hM3Dq
CNO
Virus
- + + +
+ - + +
GFP GFP GFP OX

Figure 11. DREADD-mediated upregulation of neuronal activity miR-338-3p-dependently increases GBM proliferation *in vivo.* A. Representative images of coronal cross-sections of brains stained with DAPI (grey) and injected with GFAP/tTA:TRA/hPDGFB GBM cells expressing GFP (green). **B.** 3D models of GBM created from aligned coronal serial cross-sections of allografted GBM cells expressing GFP (green), hM3Dq-mCherry-expressing cells (red) and the DAPI-stained surrounding tissue (grey), containing the cross-sections from Figure 11A. **C.** 3D reconstructions of the allografted GBM (yellow) from closed contour tracings of 3D models from Figure 11B. **D.** Mean volumes of tumors resulting from orthotopic allografts of GFAP/tTA:TRA/hPDGFB GBM cells into the murine hippocampus. No significant differences were observed between the three groups injected with cells expressing the GFP reporter ($p>0.05$). Under DREADD conditions, miR-338-3p overexpression significantly reduced tumor volume compared to control ($p<0.01$). One-way ANOVA with multiple comparisons. n=4, sham and overexpressor + DREADD; n=5, vehicle; n=6, DREADD + GFP. ns $p>0.05$, ** $p<0.01$. Results show mean ± SEM.

The hM3Dq-mCherry receptor was strongly expressed local to the tumor and within the hippocampus in all relevant groups, and the sham group displayed no corresponding fluorescence (Figure 11A). The hM3Dq-mCherry receptor was expressed over the entire length of the tumor, in most cases (Figure 11B-C, middle and right columns). Tumors maintained the same general morphology as in the prior experiment, but with less robust characteristics due to the lower average volume, which prevents more complex emergent features from manifesting.

GBM incubated in the presence of CNO without hM3Dq expression in surrounding cells had an mean volume of $8.69 \pm 5.88 \times 10^7$ μm^3, while the other control group expressing the hM3Dq receptor in the surrounding cells but injected with the vehicle had a mean GBM volume of $1.91 \pm 0.75 \times 10^8$ μm^3 (Figure 11D). The mean volumes of these two control groups did not significantly differ from one another, indicating exposure to neither CNO nor the hM3Dq receptor alone had an effect on GBM proliferation ($t_7=2.35$, $p>0.05$). In the group infected with GBM cells expressing the GFP reporter and treated with CNO, while the surrounding cells express the hM3Dq receptor,

increasing local neuronal activity, the mean GBM volume was $1.45 \pm 0.41 \times 10^8$ μm^3. This mean volume does not significantly differ from the two control groups either, indicating neuronal activity does not alter GBM proliferation *in vivo* (t_9=1.95, p>0.05). However, the group expressing the miR-338-3p overexpressor in GBM cells under the same conditions had a comparatively low mean GBM volume of $4.49 \pm 2.11 \times 10^7$ μm^3. Between the two groups exposed to entire DREADD system, the cells expressing the miR-338-3p overexpressor gave rise to a tumor with a significantly lower volume than the tumor arising from cells expressing the GFP reporter (t_8=4.48, p<0.01). These results indicate that either increasing neuronal activity does not upregulate GBM proliferation but miR-338-3p expression is actually sufficient to inhibit GBM proliferation *in vivo,* or that miR-338-3p inhibits GBM proliferation *in vivo* under conditions of high neuronal activity, which is not itself sufficient to induce proliferation.

Discussion

Our findings in this study demonstrate a clear regulatory role for miR-338-3p in the development and proliferation of cells in the dentate gyrus. Our study is the first to examine the effects of miR-338-3p on the morphology of dentate gyrus granule neurons. MiR-338-3p's effects on neuronal development are clearly apparent from our observations of aberrant somatodendritic morphology in miR-338-3p knockdown neurons. Granule neurons deficient in miR-338-3p throughout development tend to sprout multiple primary dendrites and subsequently branch off at deviant angles with respect to the soma. The morphological data from miR-338-3p knockdown indicate a relatively specialized role in regulating dentate gyrus granule neuron morphology, only having an influence on two closely related phenomena both related to altered dendritic sprouting. We did not expect a miRNA to have such a circumscribed role, given that miRNAs exert their effects on a general scale via small regulatory changes to a wide range of genes controlling a diverse group of phenomena.

These changes suggest that miR-338-3p could potentially regulate proteins involved in neuronal polarization and neurite formation. They could arise through miR-338-3p's inhibition of *PREX2a* expression, which is the most likely putative mechanism simply because alterations to the balance between the opposing activities of PI3K and PTEN in the Akt pathway generally control establishment of neurite polarity throughout neuronal development (Barnes and Polleux, 2009). MiR-338-3p knockdown upregulates *PREX2a* expression, inhibiting PTEN activity and producing a phenotype partially resembling *PTEN* loss-of-function in the developing granule neuron, which sprouts multiple primary dendrites in a similar fashion (Williams et al., 2015). Interestingly, this

phenotype includes drastic and diverse changes to granule morphology not observed in miR-338-3p knockdown neurons, such as increased soma size, dendritic arborization, and dendritic spine density (Williams et al., 2015). *PREX2a* overexpression throughout granule neuron development could prove instructive to determine whether these morphological changes result from loss of *PREX2a* regulation by miR-338-3p, especially if the changes remain limited to the suite observed under miR-338-3p knockdown, which could be induced through either weaker changes to PTEN activity or maintenance of the protected aspects of granule neuron morphology via repression of other proteins' expression. MiR-338-3p could also exert all of its influence on granule neuron morphology by repressing now-unknown molecular targets; if *PREX2a* does not directly induce the expected changes, finding these targets would hold the greatest promise.

Surprisingly, studies of hippocampal neuron phenotypes associated with schizophrenia in both animal models and in clinical samples have previously described both aberrant somatodendritic orientation and the presence of basal and multiple primary dendrites (Duan et al., 2007; Kvajo et al., 2008; Lauer et al., 2003; Senitz and Beckmann, 2003). Our findings further strengthen the association between loss of miR-338-3p expression and schizophrenia by observing the phenotype produced by miR-338-3p knockdown during neural development yields the same phenotype observed in schizophrenia. They also suggest a second mechanism by which loss of miR-338-3p expression can lead to schizophrenia. The only proposed mechanism thus far is that loss of miR-338-3p expression disrupts auditory thalamocortical transmission, inhibiting auditory sensorimotor gating and producing auditory hallucinations (Chun et al., 2017). Both the Disc1 and Df(16) murine schizophrenia models, which respectively exhibit

similarly altered granule neuron morphology and decreased miR-338-3p expression, display impaired corticohippocampal functional connectivity, which underlies and correlates with working memory deficits, a core cognitive symptom of schizophrenia (Chun et al., 2017; Dawson et al., 2015; Kvajo et al., 2008; Lett et al., 2014; Sigurdsson et al., 2010). Excitatory entorhinal cortex projections to the dentate gyrus onto granule neurons mediate most prefrontal input into the hippocampus, so miR-338-3p induced deficits in dentate gyrus dendritic morphology could impair working memory by producing these deficits to corticohippocampal connectivity. Performing bilateral miR-338-3p knockdown in the neonatal dentate gyrus followed by non-auditory working memory tasks in adulthood, like the T-maze or hole-board tasks, would help expand our deficient understanding of miR-338-3p's potential protective role in schizophrenia.

Next, we found miR-338-3p overexpression in GBM reduces its ability to proliferate. We first tested this hypothesis *in vitro* using miR-338-3p-deficient human GBM cells. We initially used these cells to validate the general functionality of a new miR-338-3p overexpressor construct, which was sufficient to induce near-total loss of sensor expression. We noted a significant and profound decrease in the proliferation rate of both human GBM cell lines under miR-338-3p overexpression. We observed the phenomenon in both cell lines, establishing miR-338-3p's anti-proliferative effect in GBM and reducing the likelihood that it arose from off-target cell line-specific features. This effect on *in vitro* GBM cell proliferation matches miR-338-3p's general inhibitory effect on proliferation across most other forms of cancer *in vitro* in the literature.

Despite the strength of our evidence and its corroboration with prior literature, our results run counter to a recent study where inducing miR-338-3p expression has no effect

on the proliferation of U251 cells (Wang et al., 2012). These differences could be explained by divergent methodologies. Wang *et al.* examined changes during the first 96 hours of infection, while our study began analysis 7 days after infection; differences in the time course of regulated genes' activity could underlie differences observed between the two studies. We could also explain differences based on the manner of infection: while our construct contained only the mature miR-338-3p sequence, theirs contains a longer sequence surrounding miR-338-3p as well. Regulatory elements within the sequence surrounding *MiR338* could have contributed to the different observed effects.

We were also able to confirm miR-338-3p's inhibition of GBM cell proliferation *in vivo* under increased local neuronal activity. To this end, we developed a murine hippocampal GBM model, recapitulating the putative gliomagenesis observed upon miR-338-3p knockdown in the dentate gyrus. Growth of the tumors in this model displayed a robust gross morphology, where almost all grew caudally from the injection site and assumed an oblong shape with a long rostrocaudal axis. This pattern of growth is very interesting, and lack of observed dorsoventral, mediolateral, or omnidirectional growth patterns suggests growth may be directed by one or more factors. One factor could potentially be differential septotemporal expression of trophic factors within the hippocampus. For example, BDNF is a strong glioma mitogen expressed in rodents at a higher level in the middle and ventral hippocampus than the dorsal hippocampus, which could direct glioma growth in that direction (Toyoda et al., 2014; Venkatesh et al., 2015). However, tumor growth continues into the subiculum instead of growing along the septotemporal axis, so differential septotemporal trophic factor expression may not entirely explain this robust growth pattern.

Our first experiment utilizing this GBM model simultaneously demonstrated our model's potential utility and its relatively low power. Our model clearly required more optimization before further use in our laboratory. In particular, each group displayed high within-group variance, indicating this model is very sensitive to very small deviations within the bounds of the protocol. Two future modifications, one exogenous and one endogenous to the model, stood out as potential opportunities to reduce variance in future studies using this model after its initial development. The first, endogenous modification would be to make the number of cells injected into the hippocampus more precise. Exponential growth is highly sensitive to initial conditions, and when these cells are left to proliferate exponentially, the initially small variation in the amount injected will similarly grow exponentially. To minimize variance, we could automate initial cell counts prior to injection, which removes the human error inherent to hemocytomer-based counts arising from the count itself and from the required dilutions and transfers.

We implemented the second, exogenous modification in our second experiment, where we simply increased the sample size to bring it closer to the size suggested by our power analysis. By increasing the sample size, we were able to increase the power of our test, uncovering a potential *in vivo* effect of miR-338-3p overexpression: the tumor overexpressing miR-338-3p had a much lower final volume than the comparable tumor with unmanipulated miR-338-3p expression in the presence of the DREADD system. These results agree with both our *in vitro* proliferation experiment as well as other *in vivo* experiments using multiple other methods to model multiple other types of cancer.

However, we were unable to replicate neuronal activity's proliferative effect in glioma reported elsewhere, but a few potential alternative explanations are possible

(Venkatesh et al., 2015). The first and most obvious is that the DREADD system did not increase neuronal activity, which is relatively unlikely because previous experiments performed in the laboratory using the system yield expected results, but it still warrants consideration (Skelton P.D., unpublished data). Unfortunately, our experimental design was not well suited to answer this question: hM3Dq-mCherry was diffusely expressed and insufficient to resolve neuronal phenotypes associated with increased neuronal activity (i.e. recurrent mossy fibers, ectopic hilar granule neurons). Further, we did not perform CNO infusion immediately prior to sacrifice, preventing validation via Arc or Fos quantification in hM3Dq-expressing cells. Future experiments could verify neuronal activity by expressing hM3Dq under a cell-type specific promoter like *CAMKIIα* or by performing CNO infusions immediately prior to sacrifice, allowing Arc or Fos quantification as a proxy for neuronal activity. That said, even if the DREADD system did function as intended, we still may not have been able to detect an existing effect either. The original study used grafted tumor cells too, but their cells were distributed diffusely throughout the tissue (as opposed to our model's tumor) and they quantified based on proliferation-associated biomarkers alone, not volume. The GBM model used in our study is relatively volatile; if neuronal activity only modestly or subclinically increases glioma proliferation, our model may not possess sufficient precision to detect it.

Increasing precision and statistical power may not explain all of the observed effects or the lack thereof. Of the two groups infected with the DREADD and treated with CNO, only the control's group size increased, the size of the group overexpressing miR-338-3p remained the same. While statistical power was still increased, the power was still not at the recommended level if we assume the effect size held constant in the

first and second experiments. Another factor may have increased the effect of miR-338-3p overexpression, potentially by magnifying the degree of its increase in activity and/or its expression. As stated in the introduction, neuronal activity is one of the few factors known to upregulate miR-338-3p expression (Luikart et al., 2012). Our miR-338-3p overexpressor constitutively expressed the miRNA, so such a mechanism did not act on the construct itself. Neither the GFAP/tTA:TRA/hPDGFB tumor cells nor the strain itself are proven to lack miR-338-3p expression, so activity-upregulated physiological miR-338-3p expression alongside overexpression may have synergized to magnify miR-338-3p expression and by extension, the resulting phenotype. We could perform miRNA-Seq for miR-338-3p in overexpressor-infected tumor samples from the two *in vivo* experiments, comparing miR-338-3p expression between the groups from the first and second experiments, which mostly differed in DREADD exposure. Other interesting mechanisms could also be possible outside of miR-338-3p expression differences, like neuronal activity upregulating miR-338-3p activity at the level of the miRISC, but the literature contains almost nothing about activity-dependent regulation of miRNA function outside of their transcription and cleavage throughout biogenesis (Eacker et al., 2013).

So far, a plethora of potential experiments have been proposed in this discussion, but most are highly speculative. In reality, the immediate next step would be to identify molecular targets of miR-338-3p that could potentially induce the range of these observed changes in proliferation and maturation. We would primarily focus our attention on three validated targets of miR-338-3p. The first is *PREX2a*, which could plausibly induce the morphological changes, as discussed earlier in this section, and increases proliferation in NB (Chen et al., 2013). The second is *MACC1,* the only gene upregulated in glioma due

to loss of miR-338-3p expression. *MACC1* expression, as discussed in the introduction, upregulates Akt signaling by an unknown mechanism to exert its effects on differentiation, and downregulating its expression decreases proliferation in nasopharyngeal carcinoma (Meng et al., 2013) The third is *SMO*, which primarily expresses in proliferating neural stem cells in the dentate gyrus, miR-338-3p-dependently stimulates proliferation in a variety of cancers as also discussed in the introduction, and its constitutive activity throughout neuronal development in the olfactory bulb alters dendritic orientation (Ihrie et al., 2011; Lai et al., 2003). We could alter the expression of any of these genes in the same direction that the miR-338-3p manipulation induced in each experiment, hoping to recapitulate the respective phenotypes we observed in each.

In conclusion, this study greatly enhances our understanding of miR-338-3p as a suppressor of GBM in two ways. First, we describe a novel regulatory function *in vivo* for miR-338-3p in the development of granule neurons in the dentate gyrus. Second, we observe a mechanism by which miR-338-3p suppresses GBM, inhibiting GBM proliferation both *in vitro* and *in vivo.* This study is the first in miR-338-3p to fulfill Mendell's third criterion for GBM, validating its suppression of gliomagenesis *in vivo*. Our study is the second to fulfill Mendell's fourth criterion, demonstrating two separate novel mechanisms by which miR-338-3p suppresses gliomagenesis. However, further study is still required to determine the molecular pathways responsible for these alterations, which would allow a more complete understanding of how exactly miR-338-3p protects the CNS against GBM. Our findings indicate miR-338-3p is a tumor suppressor for GBM. As we gradually learn more about miR-338-3p's ties to GBM, we hope that we could one day use it as a clinically relevant target for therapeutic gain.

References

Aldape, K., Zadeh, G., Mansouri, S., Reifenberger, G., and von Deimling, A. (2015). Glioblastoma: pathology, molecular mechanisms and markers. Acta Neuropathol. *129*, 829-848.

Alexander, G.M., Rogan, S.C., Abbas, A.I., Armbruster, B.N., Pei, Y., Allen, J.A., Nonneman, R.J., Hartmann, J., Moy, S.S., Nicolelis, M.A.*, et al.* (2009). Remote control of neuronal activity in transgenic mice expressing evolved G protein-coupled receptors. Neuron. *63*, 27-39.

Ames, H.M., Yuan, M., Vizcaino, M.A., Yu, W., and Rodriguez, F.J. (2017). MicroRNA profiling of low-grade glial and glioneuronal tumors shows an independent role for cluster 14q32.31 member miR-487b. Mod. Pathol. *30*, 204-216.

Aschrafi, A., Kar, A.N., Natera-Naranjo, O., MacGibeny, M.A., Gioio, A.E., and Kaplan, B.B. (2012). MicroRNA-338 regulates the axonal expression of multiple nuclear-encoded mitochondrial mRNAs encoding subunits of the oxidative phosphorylation machinery. Cell. Mol. Life Sci. *69*, 4017-4027.

Aschrafi, A., Schwechter, A.D., Mameza, M.G., Natera-Naranjo, O., Gioio, A.E., and Kaplan, B.B. (2008). MicroRNA-338 regulates local cytochrome c oxidase IV mRNA levels and oxidative phosphorylation in the axons of sympathetic neurons. J. Neurosci. *28*, 12581-12590.

Bader, A.G., Brown, D., Stoudemire, J., and Lammers, P. (2011). Developing therapeutic microRNAs for cancer. Gene Ther. *18*, 1121-1126.

Baek, D., Villén, J., Shin, C., Camargo, F.D., Gygi, S.P., and Bartel, D.P. (2008). The impact of microRNAs on protein output. Nature. *455*, 64-71.

Bakkar, A., Alshalalfa, M., Petersen, L.F., Abou-Ouf, H., Al-Mami, A., Hegazy, S.A., Feng, F., Alhajj, R., Bijian, K., Alaoui-Jamali, M.A.*, et al.* (2016). MicroRNA 338-3p exhibits tumor suppressor role and its down-regulation is associated with adverse clinical outcome in prostate cancer patients. Mol. Biol. Rep. *43*, 229-240.

Barik, S. (2008). An intronic microRNA silences genes that are functionally antagonistic to its host gene. Nucleic Acids Res. *36*, 5232-5241.

Barnes, A.P., and Polleux, F. (2009). Establishment of axon-dendrite polarity in developing neurons. Annu. Rev. Neurosci. *32*, 347-381.

Bartel, D.P. (2004). MicroRNAs: genomics, biogenesis, mechanism, and function. Cell. *116*, 281-297.

Baumann, V., and Winkler, J. (2014). MiRNA-based therapies: Strategies and delivery platforms for oligonucleotide and non-oligonucleotide agents. Future Med. Chem. *6*, 1967-1984.

Bernstein, E., Caudy, A.A., Hammond, S.M., and Hannon, G.J. (2001). Role for a bidentate ribonuclease in the initiation step of RNA interference. Nature. *409*, 363-366.

Beveridge, N.J., Gardiner, E., Carroll, A.P., Tooney, P.A., and Cairns, M.J. (2010). Schizophrenia is associated with an increase in cortical microRNA biogenesis. Mol. Psychiatry. *15*, 1176-1189.

Borchert, G.M., Lanier, W., and Davidson, B.L. (2006). RNA polymerase III transcribes human microRNAs. Nat. Struct. Mol. Biol. *13*, 1097-1101.

Buckingham, S.C., Campbell, S.L., Haas, B.R., Montana, V., Robel, S., Ogunrinu, T., and Sontheimer, H. (2011). Glutamate release by primary brain tumors induces epileptic activity. Nat. Med. *17*, 1269-1274.

Caramuta, S., Egyhazi, S., Rodolfo, M., Witten, D., Hansson, J., Larsson, C., and Lui, W.O. (2010). MicroRNA expression profiles associated with mutational status and survival in malignant melanoma. J. Invest. Dermatol. *130*, 2062-2070.

Chen, J.S., Liang, L.L., Xu, H.X., Chen, F., Shen, S.L., Chen, W., Chen, L.Z., Su, Q., Zhang, L.J., Bi, J.*, et al.* (2016). MiR-338-3p inhibits epithelial-mesenchymal transition and metastasis in hepatocellular carcinoma cells. Oncotarget. *7,* ePub Jun 17.

Chen, K., and Rajewsky, N. (2007). The evolution of gene regulation by transcription factors and microRNAs. Nat. Rev. Genet. *8*, 93-103.

Chen, P.Y., Manninga, H., Slanchev, K., Chien, M., Russo, J.J., Ju, J., Sheridan, R., John, B., Marks, D.S., Gaidatzis, D.*, et al.* (2005). The developmental miRNA profiles of zebrafish as determined by small RNA cloning. Genes Dev. *19*, 1288-1293.

Chen, X., Pan, M., Han, L., Lu, H., Hao, X., and Dong, Q. (2013). miR-338-3p suppresses neuroblastoma proliferation, invasion and migration through targeting PREX2a. FEBS Lett. *587*, 3729-3737.

Chiang, H.R., Schoenfeld, L.W., Ruby, J.G., Auyeung, V.C., Spies, N., Baek, D., Johnston, W.K., Russ, C., Luo, S., Babiarz, J.E.*, et al.* (2010). Mammalian microRNAs: experimental evaluation of novel and previously annotated genes. Genes Dev. *24*, 992-1009.

Chun, S., Du, F., Westmoreland, J.J., Han, S.B., Wang, Y.-D., Eddins, D., Bayazitov, I.T., Devaraju, P., Yu, J., Mellado Lagarde, M.M.*, et al.* (2017). Thalamic miR-338-3p mediates auditory thalamocortical disruption and its late onset in models of 22q11.2 microdeletion. Nat. Med. *23*, 39-48.

Dawson, N., Kurihara, M., Thomson, D.M., Winchester, C.L., McVie, A., Hedde, J.R., Randall, A.D., Shen, S., Seymour, P.A., Hughes, Z.A.*, et al.* (2015). Altered functional brain network connectivity and glutamate system function in transgenic mice expressing truncated Disrupted-in-Schizophrenia 1. Transl. Psychiatry. *5*, e569.

de Faria Jr., O., Cui, Q.-L., Bin, J., Bull, S.-J., Kennedy, T., Bar-Or, A., Antel, J., Colman, D., and Dhaunchak, A. (2012). Regulation of miRNA 219 and miRNA clusters 338 and 17-92 in oligodendrocytes. Front. Genet. *3*, ePub Mar 28.

Diao, H.J., Low, W.C., Milbreta, U., Lu, Q.R., and Chew, S.Y. (2015). Nanofiber-mediated microRNA delivery to enhance differentiation and maturation of oligodendroglial precursor cells. J. Control. Release. *208*, 85-92.

Duan, B., Hu, J., Zhang, T., Luo, X., Zhou, Y., Liu, S., Zhu, L., Wu, C., Liu, W., Chen, C.*, et al.* (2017). MiRNA-338-3p/CDK4 signaling pathway suppressed hepatic stellate cell activation and proliferation. BMC Gastroenterol. *17*, 12.

Duan, X., Chang, J.H., Ge, S., Faulkner, R.L., Kim, J.Y., Kitabatake, Y., Liu, X.B., Yang, C.H., Jordan, J.D., Ma, D.K.*, et al.* (2007). Disrupted-In-Schizophrenia 1 regulates integration of newly generated neurons in the adult brain. Cell. *130*, 1146-1158.

Dugas, J.C., Cuellar, T.L., Scholze, A., Ason, B., Ibrahim, A., Emery, B., Zamanian, J.L., Foo, L.C., McManus, M.T., and Barres, B.A. (2010). Dicer1 and miR-219 are required for normal oligodendrocyte differentiation and myelination. Neuron. *65*, 597-611.

Eacker, S.M., Dawson, T.M., and Dawson, V.L. (2013). The interplay of microRNA and neuronal activity in health and disease. Front. Cell. Neurosci. *7*, ePub Aug 27.

Ebrahimi-Barough, S., Massumi, M., Kouchesfahani, H.M., and Ai, J. (2013). Derivation of pre-oligodendrocytes from human endometrial stromal cells by using overexpression of microRNA 338. J. Mol. Neurosci. *51*, 337-343.

Fine, B., Hodakoski, C., Koujak, S., Su, T., Saal, L.H., Maurer, M., Hopkins, B., Keniry, M., Sulis, M.L., Mense, S.*, et al.* (2009). Activation of the PI3K pathway in cancer through inhibition of PTEN by exchange factor P-REX2a. Science. *325*, 1261-1265.

Fricano-Kugler, C.J., Williams, M.R., Salinaro, J.R., Li, M., and Luikart, B. (2016). Designing, packaging, and delivery of high titer CRISPR retro and lentiviruses via stereotaxic injection. J. Vis. Exp. *111*, ePub May 23.

Furnari, F.B., Fenton, T., Bachoo, R.M., Mukasa, A., Stommel, J.M., Stegh, A., Hahn, W.C., Ligon, K.L., Louis, D.N., Brennan, C.*, et al.* (2007). Malignant astrocytic glioma: genetics, biology, and paths to treatment. Genes Dev. *21*, 2683-2710.

Gaedcke, J., Grade, M., Camps, J., Sokilde, R., Kaczkowski, B., Schetter, A.J., Difilippantonio, M.J., Harris, C.C., Ghadimi, B.M., Moller, S.*, et al.* (2012). The rectal cancer microRNAome--microRNA expression in rectal cancer and matched normal mucosa. Clin. Cancer Res. *18*, 4919-4930.

Gaur, A., Jewell, D.A., Liang, Y., Ridzon, D., Moore, J.H., Chen, C., Ambros, V.R., and Israel, M.A. (2007). Characterization of microRNA expression levels and their Biological correlates in human cancer cell lines. Cancer Res. *67*, 2456.

Gregory, R.I., Yan, K.-p., Amuthan, G., Chendrimada, T., Doratotaj, B., Cooch, N., and Shiekhattar, R. (2004). The Microprocessor complex mediates the genesis of microRNAs. Nature. *432*, 235-240.

Guo, B., Liu, L., Yao, J., Ma, R., Chang, D., Li, Z., Song, T., and Huang, C. (2014). MiR-338-3p suppresses gastric cancer progression through a PTEN-AKT axis by targeting P-REX2a. Mol. Cancer Res. *12*, 313-321.

Guo, J., Dong, Q., Fang, Z., Chen, X., Lu, H., Wang, K., Yin, Y., Cai, X., Zhao, N., Chen, J.*, et al.* (2010). Identification of miRNAs that are associated with tumor metastasis in neuroblastoma. Cancer Biol. Ther. *9*, 446-452.

Harris, M.A., Yang, H., Low, B.E., Mukherje, J., Guha, A., Bronson, R.T., Shultz, L.D., Israel, M.A., and Yun, K. (2008). Cancer stem cells are enriched in the side population cells in a mouse model of glioma. Cancer Res. *68*, 10051-10059.

Hitoshi, Y., Harris, B.T., Liu, H., Popko, B., and Israel, M.A. (2008). Spinal glioma: platelet-derived growth factor B–mediated oncogenesis in the spinal cord. Cancer Res. *68*, 8507.

Howe, J.R., Li, E.S., Streeter, S.E., Rahme, G.J., Chipumuro, E., Russo, G.B., Litzky, J.F., Hills, L.B., Rodgers, K.R., Skelton, P.D.*, et al.* (2017). MiR-338-3p regulates neuronal maturation and suppresses glioblastoma proliferation. PLoS ONE. *5*, e0177661.

Huang, N., Wu, Z., Lin, L., Zhou, M., Wang, L., Ma, H., Xia, J., Bin, J., Liao, Y., and Liao, W. (2015). MiR-338-3p inhibits epithelial-mesenchymal transition in gastric cancer cells by targeting ZEB2 and MACC1/Met/Akt signaling. Oncotarget. *6*, 15222-15234.

Huang, X.H., Chen, J.S., Wang, Q., Chen, X.L., Wen, L., Chen, L.Z., Bi, J., Zhang, L.J., Su, Q., and Zeng, W.T. (2011). MiR-338-3p suppresses invasion of liver cancer cell by targeting smoothened. J. Pathol. *225*, 463-472.

Huang, X.H., Wang, Q., Chen, J.S., Fu, X.H., Chen, X.L., Chen, L.Z., Li, W., Bi, J., Zhang, L.J., Fu, Q.*, et al.* (2009). Bead-based microarray analysis of microRNA expression in hepatocellular carcinoma: miR-338 is downregulated. Hepatol. Res. *39*, 786-794.

Ihrie, R.A., Shah, J.K., Harwell, C.C., Levine, J.H., Guinto, C.D., Lezameta, M., Kriegstein, A.R., and Alvarez-Buylla, A. (2011). Persistent sonic hedgehog signaling in adult brain determines neural stem cell positional identity. Neuron. *71*, 250-262.

Jin, Y., Zhao, M., Xie, Q., Zhang, H., Wang, Q., and Ma, Q. (2015). MicroRNA-338-3p functions as tumor suppressor in breast cancer by targeting SOX4. Int. J. Oncol. *47*, 1594-1602.

Junker, A., Krumbholz, M., Eisele, S., Mohan, H., Augstein, F., Bittner, R., Lassmann, H., Wekerle, H., Hohlfeld, R., and Meinl, E. (2009). MicroRNA profiling of multiple sclerosis lesions identifies modulators of the regulatory protein CD47. Brain. *132*, 3342-3352.

Kent, O.A., and Mendell, J.T. (2006). A small piece in the cancer puzzle: microRNAs as tumor suppressors and oncogenes. Oncogene. *25*, 6188-6196.

Khvorova, A., Reynolds, A., and Jayasena, S.D. (2003). Functional siRNAs and miRNAs exhibit strand bias. Cell. *115*, 209-216.

Kim, J., Krichevsky, A., Grad, Y., Hayes, G.D., Kosik, K.S., Church, G.M., and Ruvkun, G. (2004). Identification of many microRNAs that copurify with polyribosomes in mammalian neurons. Proc. Nat. Acad. Sci. U.S.A. *101*, 360-365.

Kodahl, A.R., Zeuthen, P., Binder, H., Knoop, A.S., and Ditzel, H.J. (2014). Alterations in circulating miRNA levels following early-stage Estrogen Receptor-positive breast cancer resection in post-menopausal women. PLoS ONE. *9*, e101950.

Kos, A., Klein-Gunnewiek, T., Meinhardt, J., Loohuis, N.F., van Bokhoven, H., Kaplan, B.B., Martens, G.J., Kolk, S.M., and Aschrafi, A. (2016). MicroRNA-338 attenuates cortical neuronal outgrowth by modulating the expression of axon guidance genes. Mol. Neurobiol. *53*, ePub May 14.

Kos, A., Olde Loohuis, N.F.M., Wieczorek, M.L., Glennon, J.C., Martens, G.J.M., Kolk, S.M., and Aschrafi, A. (2012). A potential regulatory role for intronic microRNA-338-3p for its host gene encoding Apoptosis-Associated Tyrosine Kinase. PLoS ONE. *7*, e31022.

Kosik, K.S. (2006). The neuronal microRNA system. Nat. Rev. Neurosci. *7*, 911-920.

Krashes, M.J., Koda, S., Ye, C., Rogan, S.C., Adams, A.C., Cusher, D.S., Maratos-Flier, E., Roth, B.L., and Lowell, B.B. (2011). Rapid, reversible activation of AgRP neurons drives feeding behavior in mice. J. Clin. Invest. *121*, 1424-1428.

Kvajo, M., McKellar, H., Arguello, P.A., Drew, L.J., Moore, H., MacDermott, A.B., Karayiorgou, M., and Gogos, J.A. (2008). A mutation in mouse Disc1 that models a schizophrenia risk allele leads to specific alterations in neuronal architecture and cognition. Proc. Natl. Acad. Sci. U.S.A. *105*, 7076-7081.

Lai, K., Kaspar, B.K., Gage, F.H., and Schaffer, D.V. (2003). Sonic hedgehog regulates adult neural progenitor proliferation in vitro and in vivo. Nat. Neurosci. *6*, 21-27.

Landgraf, P., Rusu, M., Sheridan, R., Sewer, A., Iovino, N., Aravin, A., Pfeffer, S., Rice, A., Kamphorst, A.O., Landthaler, M.*, et al.* (2007). A mammalian microRNA expression atlas based on small RNA library sequencing. Cell. *129*, 1401-1414.

Larue, L., and Bellacosa, A. (2005). Epithelial-mesenchymal transition in development and cancer: role of phosphatidylinositol 3' kinase/AKT pathways. Oncogene. *24*, 7443-7454.

Lau, N.C., Lim, L.P., Weinstein, E.G., and Bartel, D.P. (2001). An abundant class of tiny RNAs with probable regulatory roles in Caenorhabditis elegans. Science. *294*, 858-862.

Lau, P., Verrier, J.D., Nielsen, J.A., Johnson, K.R., Notterpek, L., and Hudson, L.D. (2008). Identification of dynamically regulated microRNA and mRNA networks in developing oligodendrocytes. J. Neurosci. *28*, 11720-11730.

Lauer, M., Beckmann, H., and Senitz, D. (2003). Increased frequency of dentate granule cells with basal dendrites in the hippocampal formation of schizophrenics. Psychiatry Res. Neuroimaging. *122*, 89-97.

Lavon, I., Zrihan, D., Granit, A., Einstein, O., Fainstein, N., Cohen, M.A., Cohen, M.A., Zelikovitch, B., Shoshan, Y., Spektor, S.*, et al.* (2010). Gliomas display a microRNA expression profile reminiscent of neural precursor cells. Neuro Oncol. *12*, 422-433.

Lee, R.C., and Ambros, V. (2001). An extensive class of small RNAs in Caenorhabditis elegans. Science. *294*, 862-864.

Lee, R.C., Feinbaum, R.L., and Ambros, V. (1993). The C. elegans heterochronic gene lin-4 encodes small RNAs with antisense complementarity to lin-14. Cell. *75*, 843-854.

Lee, Y., Ahn, C., Han, J., Choi, H., Kim, J., Yim, J., Lee, J., Provost, P., Radmark, O., Kim, S.*, et al.* (2003). The nuclear RNase III Drosha initiates microRNA processing. Nature. *425*, 415-419.

Lee, Y., Kim, M., Han, J., Yeom, K.-H., Lee, S., Baek, S.H., and Kim, V.N. (2004). MicroRNA genes are transcribed by RNA polymerase II. EMBO J. *23*, 4051-4060.

Lett, T.A., Voineskos, A.N., Kennedy, J.L., Levine, B., and Daskalakis, Z.J. (2014). Treating working memory deficits in schizophrenia: A review of the neurobiology. Biol. Psychiatry. *75*, 361-370.

Li, P., Chen, X., Su, L., Li, C., Zhi, Q., Yu, B., Sheng, H., Wang, J., Feng, R., Cai, Q.*, et al.* (2013). Epigenetic silencing of miR-338-3p contributes to tumorigenicity in gastric cancer by targeting SSX2IP. PLoS ONE. *8*, e66782.

Li, X., Zhang, Y., Zhang, Y., Ding, J., Wu, K., and Fan, D. (2010). Survival prediction of gastric cancer by a seven-microRNA signature. Gut. *59*, 579-585.

Lin, R.J., Xiao, D.W., Liao, L.D., Chen, T., Xie, Z.F., Huang, W.Z., Wang, W.S., Jiang, T.F., Wu, B.L., Li, E.M.*, et al.* (2012). MiR-142-3p as a potential prognostic biomarker for esophageal squamous cell carcinoma. J. Surg. Oncol. *105*, 175-182.

Liu, C., Wang, Z., Wang, Y., and Gu, W. (2015). MiR-338 suppresses the growth and metastasis of OSCC cells by targeting NRP1. Mol. Cell. Biochem. *398*, 115-122.

Liu, J., Carmell, M.A., Rivas, F.V., Marsden, C.G., Thomson, J.M., Song, J.-J., Hammond, S.M., Joshua-Tor, L., and Hannon, G.J. (2004). Argonaute2 is the catalytic engine of mammalian RNAi. Science. *305*, 1437.

Louis, D.N., Perry, A., Reifenberger, G., von Deimling, A., Figarella-Branger, D., Cavenee, W.K., Ohgaki, H., Wiestler, O.D., Kleihues, P., and Ellison, D.W. (2016). The 2016 World Health Organization classification of tumors of the central nervous system: a summary. Acta Neuropathol. *131*, 803-820.

Luch, A. (2005). Nature and nurture - lessons from chemical carcinogenesis. Nat. Rev. Cancer. *5*, 113-125.

Luikart, B.W., Bensen, A.L., Washburn, E.K., Perederiy, J.V., Su, K.G., Li, Y., Kernie, S.G., Parada, L.F., and Westbrook, G.L. (2011). MiR-132 mediates the integration of newborn neurons into the adult dentate gyrus. PLoS ONE. *6*, e19077.

Luikart, B.W., Perederiy, J.V., and Westbrook, G.L. (2012). Dentate gyrus neurogenesis, integration and microRNAs. Behav. Brain Res. *227*, 348-355.

Lund, E., Güttinger, S., Calado, A., Dahlberg, J.E., and Kutay, U. (2004). Nuclear export of microRNA precursors. Science. *303*, 95.

Maclellan, S.A., Lawson, J., Baik, J., Guillaud, M., Poh, C.F., and Garnis, C. (2012). Differential expression of miRNAs in the serum of patients with high-risk oral lesions. Cancer Med. *1*, 268-274.

Marshall, C.J. (1991). Tumor suppressor genes. Cell. *64*, 313-326.

Matthay, K.K., Maris, J.M., Schleiermacher, G., Nakagawara, A., Mackall, C.L., Diller, L., and Weiss, W.A. (2016). Neuroblastoma. Nat. Rev. Dis. Primers. *2*, 16078.

Meng, F., Li, H., Shi, H., Yang, Q., Zhang, F., Yang, Y., Kang, L., Zhen, T., Dai, S., Dong, Y*., et al.* (2013). MACC1 down-regulation inhibits proliferation and tumourigenicity of nasopharyngeal carcinoma cells through Akt/ β -Catenin signaling pathway. PLoS ONE *8*, e60821.

Moen, E.L., Fricano-Kugler, C.J., Luikart, B.W., and O?Malley, A.J. (2016). Analyzing clustered data: Why and how to account for multiple observations nested within a study participant? PLoS ONE. *11*, e0146721.

Moreau, M.P., Bruse, S.E., David-Rus, R., Buyske, S., and Brzustowicz, L.M. (2011). Altered microRNA expression profiles in postmortem brain samples from individuals with schizophrenia and bipolar disorder. Biol. Psychiatry. *69*, 188-193.

Nie, H., Li, J., Yang, X.M., Cao, Q.Z., Feng, M.X., Xue, F., Wei, L., Qin, W., Gu, J., Xia, Q*., et al.* (2015). Mineralocorticoid receptor suppresses cancer progression and the Warburg effect by modulating the miR-338-3p-PKLR axis in hepatocellular carcinoma. Hepatology. *62*, 1145-1159.

Nishimura, S., and Sekiya, T. (1987). Human cancer and cellular oncogenes. Biochem. J. *243*, 313-327.

Parent, J.M. (2007). Adult neurogenesis in the intact and epileptic dentate gyrus. In Progress in Brain Research, E.S. Helen, ed. (Elsevier), pp. 529-817.

Pasquinelli, A.E. (2012). MicroRNAs and their targets: recognition, regulation and an emerging reciprocal relationship. Nat. Rev. Genet. *13*, 271-282.

Peng, Y., Liu, Y.-M., Li, L.-C., Wang, L.-L., and Wu, X.-L. (2014). MicroRNA-338 inhibits growth, invasion and metastasis of gastric cancer by targeting NRP1 expression. PLoS ONE. *9*, e94422.

Ragusa, M., Majorana, A., Banelli, B., Barbagallo, D., Statello, L., Casciano, I., Guglielmino, M.R., Duro, L.R., Scalia, M., Magro, G*., et al.* (2010). MIR152, MIR200B, and MIR338, human positional and functional neuroblastoma candidates, are involved in neuroblast differentiation and apoptosis. J. Mol. Med. *88*, 1041-1053.

Rao, S.A.M., Santosh, V., and Somasundaram, K. (2010). Genome-wide expression profiling identifies deregulated miRNAs in malignant astrocytoma. Mod. Pathol. *23*, 1404-1417.

Reinhart, B.J., Slack, F.J., Basson, M., Pasquinelli, A.E., Bettinger, J.C., Rougvie, A.E., Horvitz, H.R., and Ruvkun, G. (2000). The 21-nucleotide let-7 RNA regulates developmental timing in Caenorhabditis elegans. Nature. *403*, 901-906.

Scapoli, L., Palmieri, A., Lo Muzio, L., Pezzetti, F., Rubini, C., Girardi, A., Farinella, F., Mazzotta, M., and Carinci, F. (2010). MicroRNA expression profiling of oral carcinoma identifies new markers of tumor progression. Int. J. Immunopathol. Pharmacol. *23*, 1229-1234.

Selbach, M., Schwanhausser, B., Thierfelder, N., Fang, Z., Khanin, R., and Rajewsky, N. (2008). Widespread changes in protein synthesis induced by microRNAs. Nature. *455*, 58-63.

Senitz, D., and Beckmann, H. (2003). Granule cells of the dentate gyrus with basal and recurrent dendrites in schizophrenic patients and controls. A comparative Golgi study. J. Neural. Transm. *110*, 317-326.

Shan, Y., Li, X., You, B., Shi, S., Zhang, Q., and You, Y. (2015). MicroRNA-338 inhibits migration and proliferation by targeting hypoxia-induced factor 1alpha in nasopharyngeal carcinoma. Oncol. Rep. *34*, 1943-1952.

Shang, C., Hong, Y., Guo, Y., and Xue, Y.-x. (2016). Mir-338-3p inhibits malignant biological behaviors of glioma cells by targeting MACC1 gene. Med. Sci. Monit. *22*, 710-716.

Sigurdsson, T., Stark, K.L., Karayiorgou, M., Gogos, J.A., and Gordon, J.A. (2010). Impaired hippocampal-prefrontal synchrony in a genetic mouse model of schizophrenia. Nature. *464*, 763-767.

Smith, K.S., Bucci, D.J., Luikart, B.W., and Mahler, S.V. (2016). DREADDS: Use and application in behavioral neuroscience. Behav. Neurosci. *130*, 137-155.

Smrt, R.D., Szulwach, K.E., Pfeiffer, R.L., Li, X., Guo, W., Pathania, M., Teng, Z.-Q., Luo, Y., Peng, J., Bordey, A.*, et al.* (2010). MicroRNA miR-137 regulates neuronal maturation by targeting ubiquitin ligase Mind Bomb-1. Stem Cells. *28*, 1060-1070.

Stark, K.L., Xu, B., Bagchi, A., Lai, W.-S., Liu, H., Hsu, R., Wan, X., Pavlidis, P., Mills, A.A., Karayiorgou, M.*, et al.* (2008). Altered brain microRNA biogenesis contributes to phenotypic deficits in a 22q11-deletion mouse model. Nat. Genet. *40*, 751-760.

Stefani, G., and Slack, F.J. (2008). Small non-coding RNAs in animal development. Nat. Rev. Mol. Cell Biol. *9*, 219-230.

Sun, E., and Shi, Y. (2015). MicroRNAs: Small molecules with big roles in neurodevelopment and diseases. Exp. Neurol. *268*, 46-53.

Sun, J., Feng, X., Gao, S., and Xiao, Z. (2015). microRNA-338-3p functions as a tumor suppressor in human nonsmallcell lung carcinoma and targets Ras-related protein 14. Mol. Med. Rep. *11*, 1400-1406.

Sun, K., Deng, H.-J., Lei, S.-T., Dong, J.-Q., and Li, G.-X. (2013). miRNA-338-3p suppresses cell growth of human colorectal carcinoma by targeting smoothened. World J. Gastroenterol. *19*, 2197-2207.

Teicher, B.A. (2006). Tumor models for efficacy determination. Mol. Cancer Ther. *5*, 2435.

The Genotype-Tissue Expression Consortium. (2013). The Genotype-Tissue Expression (GTEx) project. Nat. Genet. *45*, 580-585.

Tong, D., Zhao, L., He, K., Sun, H., Cai, D., Ni, L., Sun, R., Chang, S., Song, T., and Huang, C. (2016). MECP2 promotes the growth of gastric cancer cells by suppressing miR-338-mediated antiproliferative effect. Oncotarget. *7*, 34845-34859.

Toyoda, A., Iio, W., Goto, T., Koike, H., and Tsukahara, T. (2014). Differential expression of genes encoding neurotrophic factors and their receptors along the septal-temporal axis of the rat hippocampus. Anim. Sci. J. *85*, 986-993.

Tsuchiya, S., Oku, M., Imanaka, Y., Kunimoto, R., Okuno, Y., Terasawa, K., Sato, F., Tsujimoto, G., and Shimizu, K. (2009). MicroRNA-338-3p and microRNA-451 contribute to the formation of basolateral polarity in epithelial cells. Nucleic Acids Res. *37*, 3821-3827.

Vargas, J.N., Kar, A.N., Kowalak, J.A., Gale, J.R., Aschrafi, A., Chen, C.Y., Gioio, A.E., and Kaplan, B.B. (2016). Axonal localization and mitochondrial association of precursor microRNA 338. Cell. Mol. Life Sci. *73*, 4327-4340.

Venkatesh, Humsa S., Johung, Tessa B., Caretti, V., Noll, A., Tang, Y., Nagaraja, S., Gibson, Erin M., Mount, Christopher W., Polepalli, J., Mitra, Siddhartha S.*, et al.* (2015). Neuronal activity promotes glioma growth through Neuroligin-3 secretion. Cell. *161*, 803-816.

Wang, L., Shi, M., Hou, S., Ding, B., Liu, L., Ji, X., Zhang, J., and Deng, Y. (2012). MiR-483–5p suppresses the proliferation of glioma cells via directly targeting ERK1. FEBS Lett. *586*, 1312-1317.

Weber, M.J. (2005). New human and mouse microRNA genes found by homology search. FEBS J. *272*, 59-73.

Weller, M., Wick, W., Aldape, K., Brada, M., Berger, M., Pfister, S.M., Nishikawa, R., Rosenthal, M., Wen, P.Y., Stupp, R.*, et al.* (2015). Glioma. Nat. Rev. Dis. Primers. *1*, 15017.

Wightman, B., Ha, I., and Ruvkun, G. (1993). Posttranscriptional regulation of the heterochronic gene lin-14 by lin-4 mediates temporal pattern formation in C. elegans. Cell. *75*, 855-862.

Williams, M.R., DeSpenza, T., Jr., Li, M., Gulledge, A.T., and Luikart, B.W. (2015). Hyperactivity of newborn Pten knock-out neurons results from increased excitatory synaptic drive. J. Neurosci. *35*, 943-959.

Winter, J., Jung, S., Keller, S., Gregory, R.I., and Diederichs, S. (2009). Many roads to maturity: microRNA biogenesis pathways and their regulation. Nat. Cell Biol. *11*, 228-234.

Wu, B., Li, C., Zhang, P., Yao, Q., Wu, J., Han, J., Liao, L., Xu, Y., Lin, R., Xiao, D.*, et al.* (2013). Dissection of miRNA-miRNA interaction in esophageal squamous cell carcinoma. PLoS ONE. *8*, e73191.

Wu, X.-m., Shao, X.-q., Meng, X.-x., Zhang, X.-n., Zhu, L., Liu, S.-x., Lin, J., and Xiao, H.-s. (2011). Genome-wide analysis of microRNA and mRNA expression signatures in hydroxycamptothecin-resistant gastric cancer cells. Acta Pharmacol. Sin. *32*, 259-269.

Xu, H., Zhao, L., Fang, Q., Sun, J., Zhang, S., Zhan, C., Liu, S., and Zhang, Y. (2014). MiR-338-3p Inhibits Hepatocarcinoma Cells and Sensitizes These Cells to Sorafenib by Targeting Hypoxia-Induced Factor 1 α . PLoS ONE. *9*, e115565.

Xue, Q., Sun, K., Deng, H.-J., Lei, S.-T., Dong, J.-Q., and Li, G.-X. (2014). MicroRNA-338-3p Inhibits Colorectal Carcinoma Cell Invasion and Migration by Targeting Smoothened. Jpn. J. Clin. Oncol. *44*, 13-21.

Yan, Y., Fan, Q., Wang, L., Zhou, Y., Li, J., and Zhou, K. (2017). LncRNA Snhg1, a non-degradable sponge for miR-338, promotes expression of proto-oncogene CST3 in primary esophageal cancer cells. Oncotarget. *8*, ePub Mar 14.

Yang, M., Liu, R., Sheng, J., Liao, J., Wang, Y., Pan, E., Guo, W., Pu, Y., and Yin, L. (2013). Differential expression profiles of microRNAs as potential biomarkers for the early diagnosis of esophageal squamous cell carcinoma. Oncol. Rep. *29*, 169-176.

Yue, J., Sheng, Y., and Orwig, K.E. (2008). Identification of novel homologous microRNA genes in the rhesus macaque genome. BMC Genom. *9*, 8.

Zhang, B., Pan, X., Cobb, G.P., and Anderson, T.A. (2007). microRNAs as oncogenes and tumor suppressors. Dev. Biol. *302*, 1-12.

Zhang, G., Zheng, H., Zhang, G., Cheng, R., Lu, C., Guo, Y., and Zhao, G. (2017). MicroRNA-338-3p suppresses cell proliferation and induces apoptosis of non-small-cell lung cancer by targeting sphingosine kinase 2. Cancer Cell Int. *17*, 46.

Zhang, M., Wang, W., Li, T., Yu, X., Zhu, Y., Ding, F., Li, D., and Yang, T. (2016a). Long noncoding RNA SNHG1 predicts a poor prognosis and promotes hepatocellular carcinoma tumorigenesis. Biomed. Pharmacol. *80*, 73-79.

Zhang, T., Liu, W., Zeng, X.-c., Jiang, N., Fu, B.-s., Guo, Y., Yi, H.-m., Li, H., Zhang, Q., Chen, W.-j.*, et al.* (2016b). Down-regulation of microRNA-338-3p promoted angiogenesis in hepatocellular carcinoma. Biomed. Pharmacol. *84*, 583-591.

Zhang, Y., Shi, B., Chen, J., Hu, L., and Zhao, C. (2016c). MiR-338-3p targets pyruvate kinase M2 and affects cell proliferation and metabolism of ovarian cancer. Am. J. Transl. Res. *8*, 3266-3273.

Zhang, Y., Xie, R.L., Croce, C.M., Stein, J.L., Lian, J.B., van Wijnen, A.J., and Stein, G.S. (2011). A program of microRNAs controls osteogenic lineage progression by targeting transcription factor Runx2. Proc. Natl. Amer. Sci. U.S.A. *108*, 9863-9868.

Zhao, X., He, X., Han, X., Yu, Y., Ye, F., Chen, Y., Hoang, T., Xu, X., Mi, Q.-S., Xin, M.*, et al.* (2010). MicroRNA-mediated control of oligodendrocyte differentiation. Neuron. *65*, 612-626.